INL/RPT-22-70396-Revision-0

HYBRID Modeling of DETAIL Experimental Facility

November 2022

Daniel Mark Mikkelson, Amey Shigrekar, Aaron S Epiney, An Ho, Scott Greenwood, Konor L Frick

Changing the World's Energy Future

Idaho National Laboratory

INL is a U.S. Department of Energy National Laboratory operated by Battelle Energy Alliance, LLC

INL/RPT-22-70396-Revision-0

HYBRID Modeling of DETAIL Experimental Facility

Daniel Mark Mikkelson, Amey Shigrekar, Aaron S Epiney, An Ho, Scott Greenwood, Konor L Frick

November 2022

Idaho National Laboratory
Idaho Falls, Idaho 83415

http://www.inl.gov

Prepared for the
U.S. Department of Energy
Under DOE Idaho Operations Office
Contract DE-AC07-05ID14517

INL/RPT-22-70396
Revision 0

HYBRID Modeling of the DETAIL Experimental Facility

November | 2022

An Ho, Amey Shigrekar, Daniel Mikkelson,
Scott Greenwood, Konor L Frick, Aaron Epiney

Idaho National Laboratory

IES
Integrated Energy Systems

INL is a U.S. Department of Energy National Laboratory operated by Battelle Energy Alliance, LLC

INL/RPT-22-70396
Revision 0

HYBRID Modeling of the DETAIL Experimental Facility

**An Ho, Amey Shigrekar, Daniel Mikkelson,
Scott Greenwood, Konor L Frick, Aaron Epiney**

November | 2022

**Idaho National Laboratory
Integrated Energy Systems
Idaho Falls, Idaho 83415**

http://www.ies.inl.gov

**Prepared for the
U.S. Department of Energy
Office of Nuclear Energy
Under DOE Idaho Operations Office
Contract DE-AC07-05ID14517**

Page intentionally left blank

ABSTRACT

Idaho National Laboratory (INL) continues to be at the forefront of advanced reactor systems and integrated energy systems (IES) research. The Thermal Energy Distribution System (TEDS) and Microreactor Agile Non-nuclear Test Bed (MAGNET) experiments in the Dynamic Energy Transport and Innovation Laboratory (DETAIL) within INL's Engineering Systems Laboratory involve a mix of digital and physical testing systems that can be used to explore the operation of thermally and electrically integrated systems. Modeling of these systems has been accomplished using the IES program's HYBRID modeling repository. DETAIL also contains high-temperature steam electrolysis (HTSE) units to produce hydrogen and generate the load imposed on MAGNET and TEDS. The dynamic modeling capabilities within the IES program describe the DETAIL components as built, and can be used to evaluate controls, process flows, and overall system conditions.

Page intentionally left blank

CONTENTS

FIGURES

TABLES

Page intentionally left blank

LIST OF ACRONYMS

DETAIL	Dynamic Energy Transport and Innovation Laboratory
FORCE	Framework for Optimization of ResourCes and Economics
HTSE	High-temperature steam electrolysis
IES	Integrated energy systems
INL	Idaho National Laboratory
MAGNET	Microreactor Agile Non-nuclear Test Bed
OCV	Open circuit voltage
PCU	Power Conversion Unit
PI	Proportional integral
PID	Proportional integral derivative
SOEC	Solid oxide electrolytic cell
TEDS	Thermal Energy Distribution System
TES	Thermal energy storage

Page intentionally left blank

1. INTRODUCTION

Idaho National Laboratory (INL) is the host laboratory for the Integrated Energy Systems (IES) program, which seeks more efficient—and potentially more economic—methods of using carbon-free heat from nuclear power in non-electric applications. To support this research, laboratory facilities have been constructed that can integrate real-time digital signals, mock nuclear power, thermal energy storage (TES), and industrial heat use via high-temperature electrolysis. The Dynamic Energy Technology and Integration Laboratory (DETAIL), seen in Figure 1, houses the Microreactor Agile Non-nuclear Experimental Test Bed (MAGNET) and the Thermal Energy Distribution System (TEDS). MAGNET houses an electrical heating element that enables it to simulate nuclear reactor cores with microreactor test elements inside the environmental chamber, while TEDS contains a thermocline TES system. MAGNET and TEDS are thermally integrated via a heat exchanger.

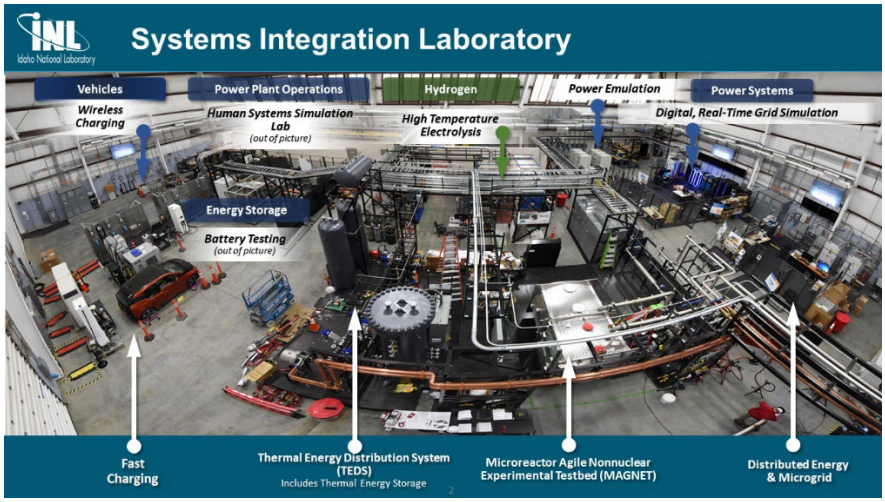

Figure 1. Wide view of the Systems Integration Laboratory, which contains the DETAIL facility.

The IES team continues to create dynamic models using Modelica, an open-source and equation-based acausal language for engineering applications. Under the IES program, integration of Modelica modeling into the HYBRID repository has been underway since 2013. Modelica has been the language of choice due to its object-oriented construction, open-source development, and inherently dynamic model construction. By leveraging these characteristics, HYBRID modelers can quickly develop new systems by utilizing building block structures created either internally, in the open-source Modelica Standard Library, or using Oak Ridge National Laboratory's open-source TRANSFORM library. A system-wide ramping capability, thermal and electrical integration methods, control, and feedback are observable via the HYBRID output.

As part of the engineering design process for the current experimental setup—as well as for future individual experiments—the IES team has been using HYBRID modeling repository tools to develop dynamic DETAIL models for a variety of applications, including validation and verification of the HYBRID modeling techniques, control system design, digital twinning, and real-time optimization efforts [1]. This report details the development of the MAGNET model and its integration with the existing TEDS model. Development of the HYBRID TEDS model was reported on in a previous year [2]. Additionally, initial validation and verification efforts were conducted for TEDS [3]. As the current research has not included a supplemental TEDS modeling effort, this report will not present details on the TEDS model.

The other currently designed portion of DETAIL that has been modeled within HYBRID is the high-temperature steam electrolysis (HTSE) solid oxide electrolytic cell (SOEC) stack. This model is planned to be unspecific in regard to cell materials and geometry, but capable of calculating the overarching production details of a HTSE process. This model will be complementary, within HYBRID, to a prior HTSE model [4].

Once the various subsystems are constructed, the IES team can integrate them as necessary to generate specific experiments within the DETAIL facility, thus helping demonstrate IES control and use within a scaled facility. Through digital twinning work, which is expected to utilize the models described in this report, IES will be able to demonstrate real-time optimization of system operations, based on physical feedback measurements fed into the digital twin in order to suggest control actions to be applied to the physical system.

2. MAGNET

MAGNET is an experimental design that was constructed at INL to aid in the development, demonstration, testing, and validation of various microreactor technologies and components. Electrical resistance heaters are used in MAGNET to simulate core thermal behavior, and this provides inputs for primary heat exchanger performance as well as passive decay heat removal for heat-pipe and gas-cooled microreactors. MAGNET will be integrated with TEDS as well as a 30 kWe gas turbine.

A schematic of the MAGNET process flow is shown in Figure 2. As seen in Figure 5 MAGNET is a combination of subsystems and components working in tandem via a control system. These components and subsystems include a 250 kW electrically heated core to simulate a heat source (e.g., a microreactor core), an environmental chamber, a 350 kW recuperator, a 265 kW heat rejection chiller, a compressor to control the coolant flow rate, and a series of insulated pipes. MAGNET also has several flanges for enabling future integration with TEDS and the 30 kWe gas turbine.

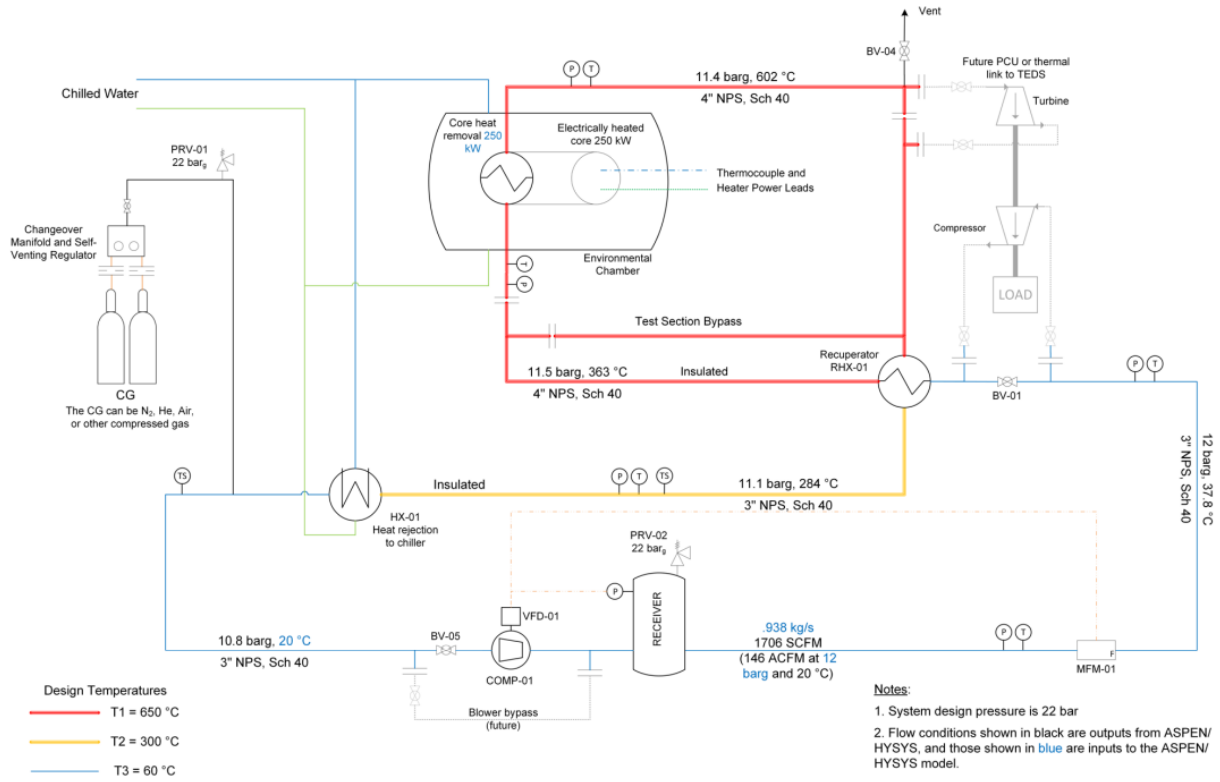

Figure 2. MAGNET process flow schematic.

2.1 Model Development

A mathematical dynamic model was created to simulate the performance of MAGNET and its integration with TEDS and the gas turbine. Using initial design data, this model was developed in the Modelica-based modeling and simulation environment [5,6]. Oak-Ridge-National-Laboratory-developed components within the TRANFORM package were also used in the model development [7]. This section describes the development of the major components of the Modelica model of MAGNET.

The coolant inside the MAGNET loop can be either compressed air, nitrogen, or helium. A steady-state process was simulated in Aspen HYSYS to determine MAGNET's nominal operating conditions. reports the primary operating temperatures of the coolant, as calculated using Aspen HYSYS. The process pressures and temperatures are reported in Figure 2. These values will be used to validate the Modelica simulation results.

As seen in both and Figure 2, the coolant is pumped into the environmental chamber at 363°C and 11.5 barg, where it is heated up by the core at a maximum rate of 250 kWth. The hot coolant exits the chamber at 602°C and passes through the recuperator to preheat the cold coolant before entering the environmental chamber. The hot coolant exits the recuperator at 284°C and 11.1 barg, and is cooled by chilled water at the heat rejection chiller. The cold coolant exits the heat rejection chiller at 20°C and 10.8 barg. A tank of compressed air, nitrogen, or helium is connected to the loop via a pressure-reducing valve. This enables control of the coolant flow rate inside the MAGNET loop. A compressor for controlling the coolant flow rate pumps the cold coolant through the recuperator so it can be preheated prior to entering the environmental chamber for reheating.

2.1.1 Heat Rejection Chiller

The heat rejection chiller was modeled as a simple counter-current heat exchanger, using the TRANSFORM heat exchanger package. The warm coolant flows through one side of the heat exchanger and is cooled by chilled water passing through the other side. The chilled water is assumed to enter at 65°F. The amount of heat rejected is determined based on the flow rate of the chilled water. The chiller uses a simple heat exchanger design whose UA value is based on MAGNET's nominal operating conditions. A schematic of the heat rejection chiller is shown in Figure 3.

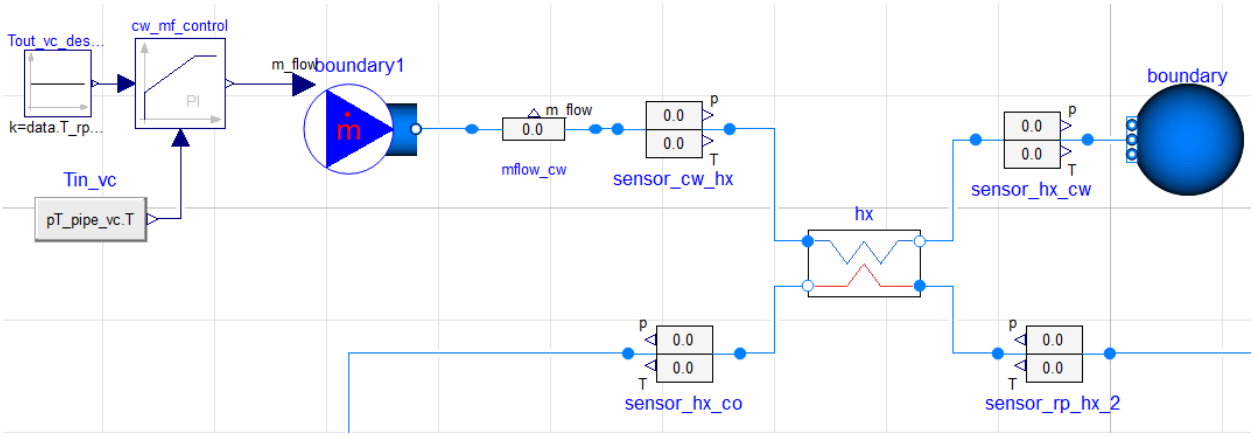

Figure 3. Heat rejection chiller schematic.

2.1.2 350 kW Recuperator

The recuperator was also modeled as a heat exchanger by using the TRANSFORM simple heat exchanger model. The hot coolant flows through one side of the heat exchanger and heats up the cold coolant flowing through the other side. The coolant flow rate is controlled via the compressor to ensure that the temperature of the coolant exiting the environmental chamber is 602°C. The recuperator design is proprietary and thus unavailable for use in the modeling. As such, the recuperator is modeled as a simple heat exchanger whose calculated average UA value is based on MAGNET's nominal operating conditions. The recuperator setup is shown in Figure 4.

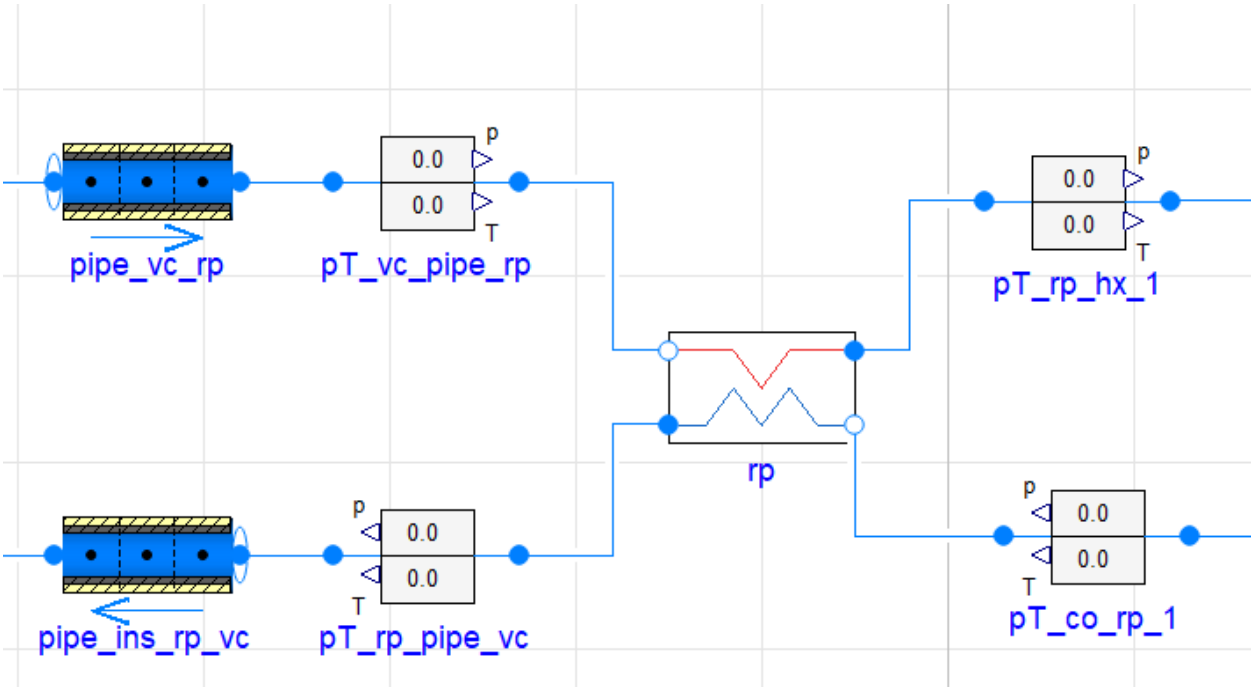

Figure 4. 350 kW recuperator schematic.

2.1.3 Control

In addition to the subsystems and components described above, a series of insulated pipes, sensors, valves, and proportional integral (PI) controllers was added to ensure the functionality of the systems working together in tandem. Figure 5 shows a full schematic of the MAGNET operational system modeled in Modelica. This section describes the controls used to maintain the operational standards pertaining to MAGNET.

As MAGNET is designed to simulate and test microreactor functions, it is desirable to maintain constant operating conditions within the microreactor core via control of system values such as inlet and outlet temperatures. The inlet temperature of the coolant entering the environmental chamber is controlled, in modeling, by regulating the chilled water flow rate at the heat rejection chiller. The chilled water flow rate is controlled by a PI controller to keep the temperature of the coolant entering the environmental chamber at 360°C. The simulation results (green) are shown in Figure 6. The PI controller attempts to minimize the error (calculated via Equation 1) between the set point temperature and the measured temperature.

$$Error_{T_{vc},in} = T_{SP,T_{vc,in}} - T_{vc,in} \quad (1)$$

If the inlet temperature of the environmental chamber is below the temperature set point, the chilled water flow rate would decrease to reduce the amount of heat being extracted, thus raising the inlet temperature. If the temperature exceeds the temperature set point, the chilled water flow rate would increase to bring the temperature back down. There is a minimum flow rate for maintaining the outlet water temperature without exceeding its boiling point. A maximum flow rate has also been implemented in the chilled water controller.

The temperature of the coolant exiting the environmental chamber is controlled by the coolant flow rate, which in turn is controlled by the compressor that pumps the coolant through the recuperator and into the environmental chamber. The results of this process are shown (in red) in Figure 6. The PI controller minimizes the temperature error calculated via Equation 2 by moderating the flow rate as needed to maintain a constant outlet temperature. This control method is used when the core power is set as an independent variable.

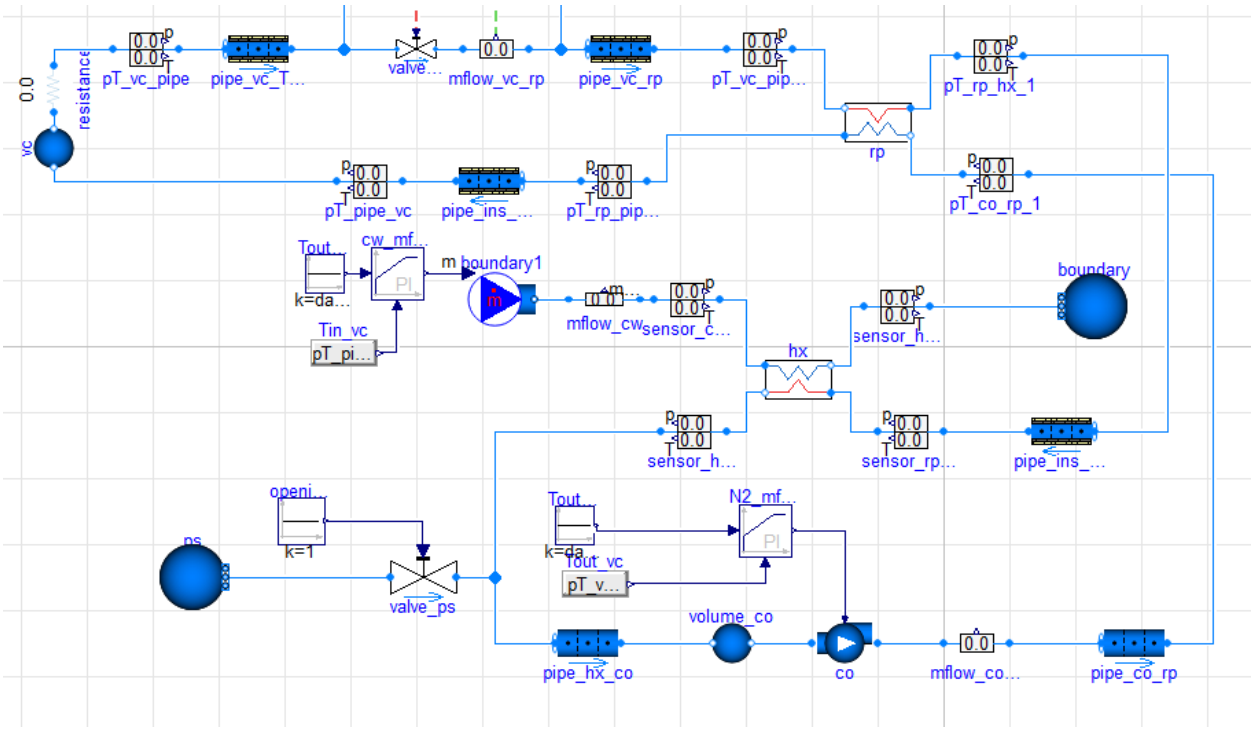

Figure 5. Heat rejection chiller schematic.

2.2 Modeling Results

2.2.1 Steady-State Operation

Steady-state simulation results were generated from the Modelica model, using the same inputs on which the Aspen HYSYS model was run. The results were then compared with those of Aspen HYSYS, using the aforementioned UA values calculated for the recuperator and the heat rejection chiller. The results are given in Table 1, and show good agreement between the two models, as the coolant flow rate is calculated to be the same as that in the HYSYS model. Furthermore, the outlet and inlet temperatures of the vaccuum chamber were within 0.1% of the Aspen HYSYS model results. The recuperator outlet temperature showed a 0.18% difference, while the inlet and outlet compressor temperatures only showed differences of 2.7% and 1.4%, respectively.

Table 1. MAGNET steady-state simulation results.

	Modelica	Aspen HYSYS	Percent Difference
Vacuum Chamber Outlet Temp	602.3°C 875.45 K	602°C 875.15 K	0.03%
Vacuum Chamber Inlet Temp	362.5°C 635.65 K	363°C 636.15 K	-0.08%
Recuperator Outlet Temp	285°C 558.15 K	284°C 557.15 K	0.18%
Compressor Inlet Temp	28°C 301.15 K	20°C 293.15 K	2.7%
Compressor Outlet Temp	42.3°C 315.45 K	37.8°C 310.95 K	1.4%
Coolant Flow Rate	0.938 kg/s	0.938 kg/s	0.00%

Some of these minor differences may be due to material package differences between the two tools. Obtaining similar results reinforces confidence in the system setup. Future efforts will use laboratory data to validate and verify these results.

2.2.2 Dynamic Operation

To evaluate the model responsiveness with respect to changes in vacuum chamber heat rate, a dynamic operation was simulated using the developed model and control scheme. A 400,000 second simulation was run to assess the system response. The heat rate began at full capacity: 250 kWth. The coolant flow rate at the beginning of the simulation started at its nominal value of 0.938 kg/s. At 50,000 seconds, the heat rate began to ramp down, reaching 70% of its full capacity at 150,000 seconds, as shown in Figure 7. The heat rate remained constant at 70% capacity until 250,000 seconds, at which point it started to ramp back up. The heat rate reached 100% capacity at 350,000 seconds, and remained at 100% through the end of the simulation.

In response to these changes in heat rate, the coolant and chilled water flow rate adjust accordingly to keep the inlet/outlet temperature of the vacuum chamber constant. These responses can be seen in Figure 7. As the heat rate began to decrease at 50,000 seconds, in order to keep the outlet temperature constant, the coolant flow rate also decreased. However, as the coolant flow rate decreased, the outlet temperature of the recuperator also decreased, as shown in Figure 6 and Figure 7. The recuperator outlet temperature lowered to 247°C as the coolant flow rate decreased to 0.723 kg/s. Similarly, the outlet temperature on the other side of the recuperator rose to 390°C (seen as the inlet temperature of the vacuum chamber in Figure 6). At most, the chilled water can only lower the temperature of the warm coolant down to the chilled water's inlet temperature. Therefore, a maximum flow rate of 2 kg/s is implemented in the chilled water control. At 350,000 seconds, the heat rate again started to rise, and the coolant flow rate increased to its nominal value. The inlet temperature of the vacuum chamber also started decreasing, reaching 360°C by 350,000 seconds and staying there until the end of the simulation, as the system remained at its full capacity.

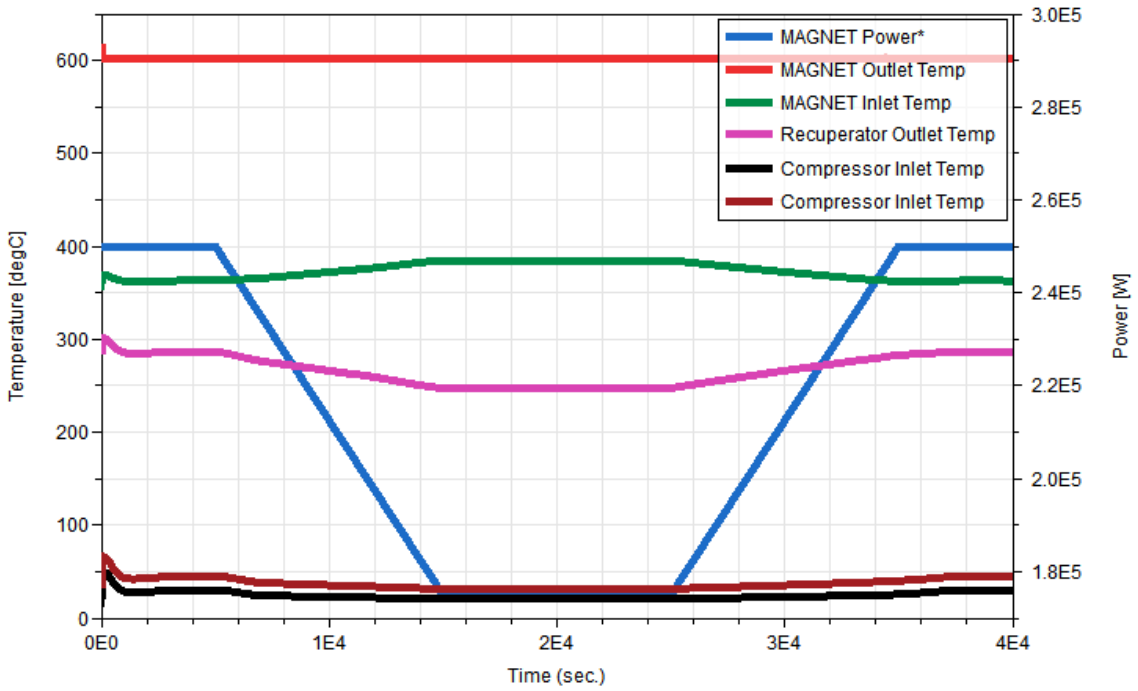

Figure 6. Temperature response to changes in heat rate.

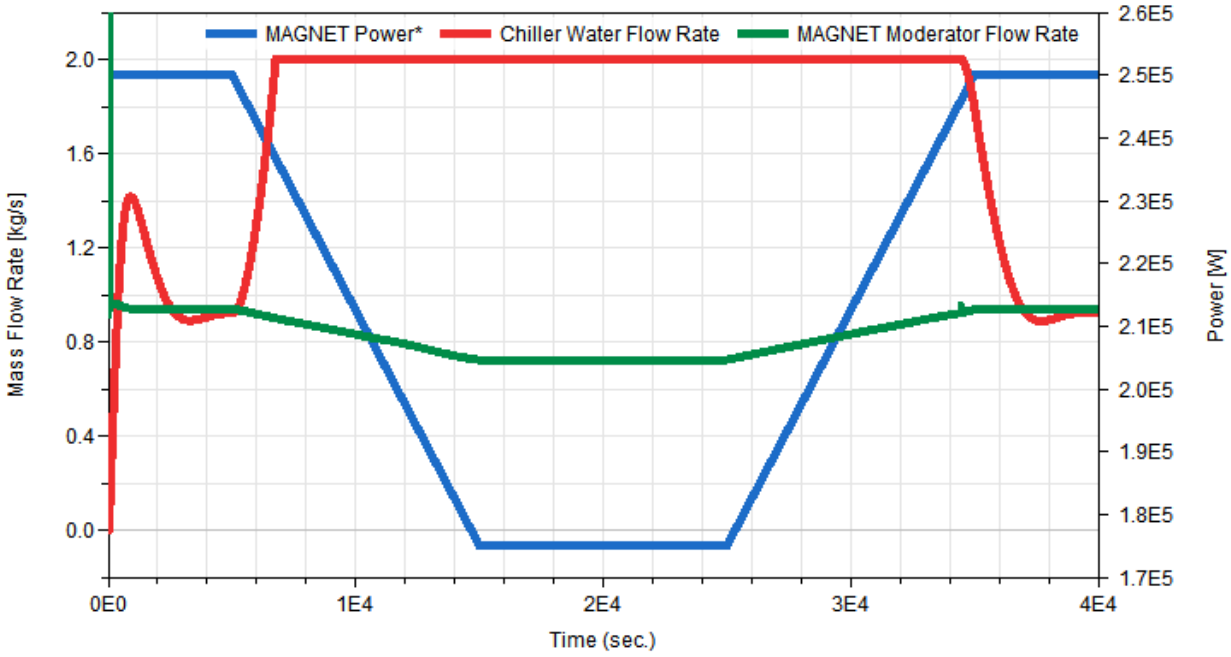

Figure 7. Coolant and chilled water flow rate response to changes in heat rate.

3. MAGNET-TEDS-PCU INTEGRATION

MAGNET was designed to be integrated with a thermal storage unit, a power conversion unit (PCU), a HTSE unit, and a synthetic fuel production unit to test and prove microreactor/hybrid technologies. The thermal storage unit is a thermocline storage unit, and the PCU is a 30 kWe gas turbine. A dynamic model integrating MAGNET, the thermocline storage unit, and the gas turbine was developed to simulate the transient process of the hybrid system in order to generate insights into the integration process, coupling mechanisms, control strategies, and system response to dynamic variations such as electricity and heat demands.

MAGNET will act as a thermal heat source, with nitrogen serving as the coolant to transport the thermal energy generated inside the vacuum chamber to the gas turbine in order to meet the electricity demand. If the thermal heat is more than what is needed to meet the electricity demand, the excess heat will be transferred to TEDS. This is accomplished through a helical coil heat exchanger that transfers the heat from MAGNET to TEDS. TEDS can use this excess heat to meet the heat demand, or can store it in the thermocline thermal storage. TEDS can also discharge the thermocline storage if the heat demand exceeds the amount of heat provided by MAGNET.

3.1 Model Development

3.1.1 Power Conversion Unit

A 30 kWe PCU model was developed for integration with MAGNET. The coolant is heated inside MAGNET's environmental chamber, then this heated fluid is expanded as it flows through the gas turbine, turning the generator to produce electricity and meet electricity demands of up to 30 kWe. The fluid is cooled and compressed back to the original pressure, then looped back into the MAGNET loop for reheating. A control valve controls the coolant flow rate into the gas turbine in order to match the electricity demand set by the market. The algorithm used to control the valve position is further described in Section 3.1.3. The gas turbine and the compressor were modeled via the TRANSFORM gas turbine and compressor model, using Equations 2–6:

$$W_{turbine} = w_{turbine}\left(H_{turb,in} - H_{turb,out}\right) \tag{2}$$

where $W_{turbine}$ is the power generated by the turbine, $H_{turb,in}$ is the inlet enthalpy of the coolant under inlet temperature/pressure conditions, and $H_{turb,out}$ is the outlet enthalpy at the outlet temperature/pressure conditions, and is calculated as:

$$H_{turb,out} = \eta_{isentropic}\left(H_{turb-out,iso} - H_{turb,in}\right) + H_{turb,in} \tag{3}$$

where $H_{turb-out,iso}$ is the isentropic (ideal) outlet enthalpy of the turbine and $\eta_{isentropic}$ is the isentropic efficiency.

$$W_{compressor} = w_{compressor}\left(H_{comp,out} - H_{comp,in}\right) \tag{4}$$

$$H_{comp,out} = \frac{1}{\eta_{isentropic}}\left(H_{comp-out,iso} - H_{comp,in}\right) + H_{comp,in} \tag{5}$$

where $W_{compressor}$ is the power needed by the compressor, $H_{comp,in}$ is the inlet enthalpy of the coolant at the inlet temperature/pressure conditions, $H_{comp,out}$ is the outlet enthalpy at the outlet temperature/pressure conditions, and $H_{comp-out,iso}$ is the isentropic (ideal) outlet enthalpy of the compressor.

The total power generated by the PCU can be calculated as:

$$W_{PCU} = \eta_{mech}(W_{turbine} - W_{compressor}) \tag{6}$$

where W_{PCU} is the total power generated by the PCU and η_{mech} is the mechanical efficiency. A diagram of the PCU is shown in Figure 8.

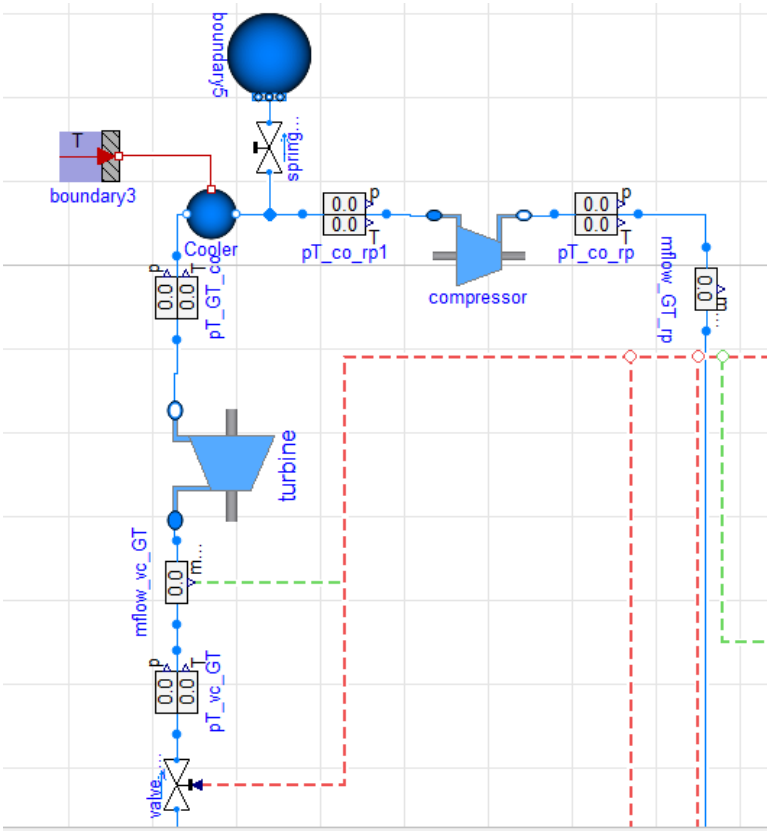

Figure 8. Power conversion unit diagram.

3.1.2 Helical Coil Heat Exchanger For Transferring Heat from MAGNET to TEDS

A helical-coil heat exchanger is used to transfer heat from MAGNET to TEDS (see Figure 9). The design of this heat exchanger is proprietary and thus unavailable for use in the modeling. Instead, a simple heat exchanger model with a calculated average UA value from the TRANSFORM package was used to model the heat exchanger. The heat exchanger was designed to ensure that the Therminol®-66 fluid inside TEDS is heated from its cold temperature to its designed hot temperature.

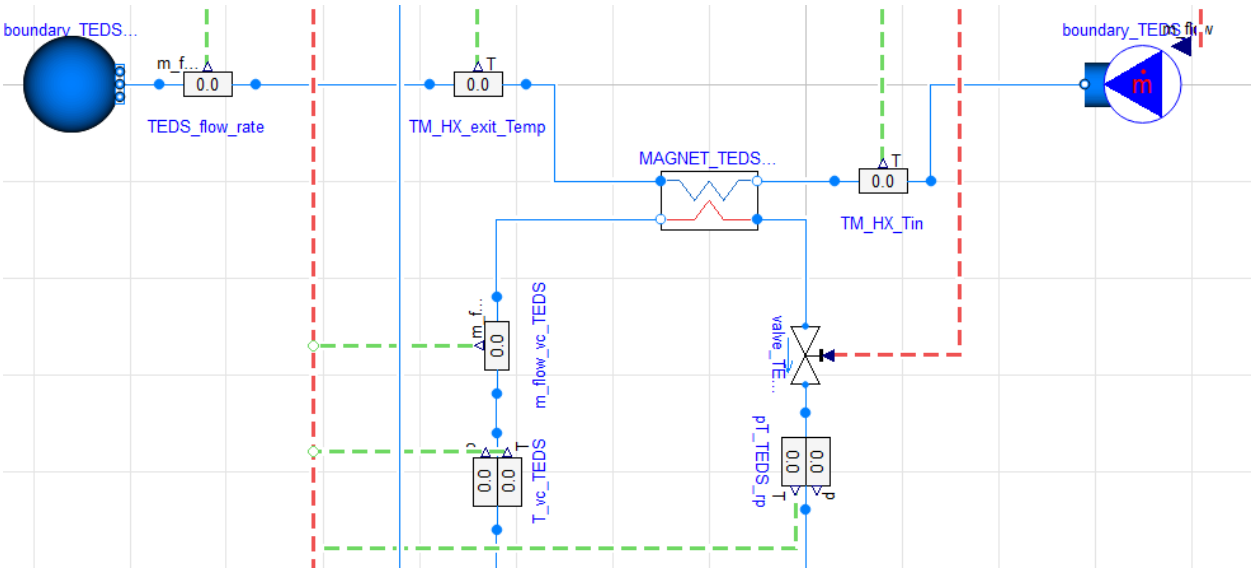

Figure 9. MAGNET-TEDS heat exchanger schematic.

3.1.3 Control

Several valves, sensors, and control algorithms are also needed to operate the hybrid system in all operating modes, and to ensure that the different components can work together within their individual operating limits. A schematic of the integration of MAGNET, TEDS, and the PCU is shown in Figure 10. A pictorial overview of the centralized control unit is shown in Figure 11. This section gives an in-depth description of the centralized control unit and its control algorithm.

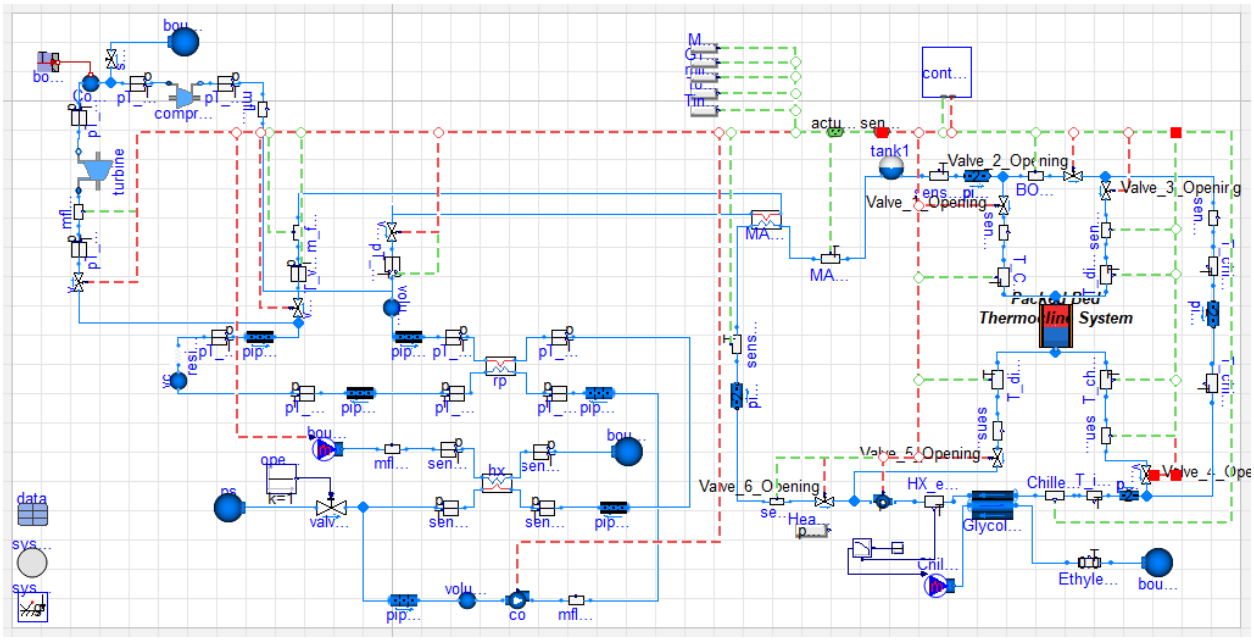

Figure 10. MAGNET-TEDS-PCU integration schematic.

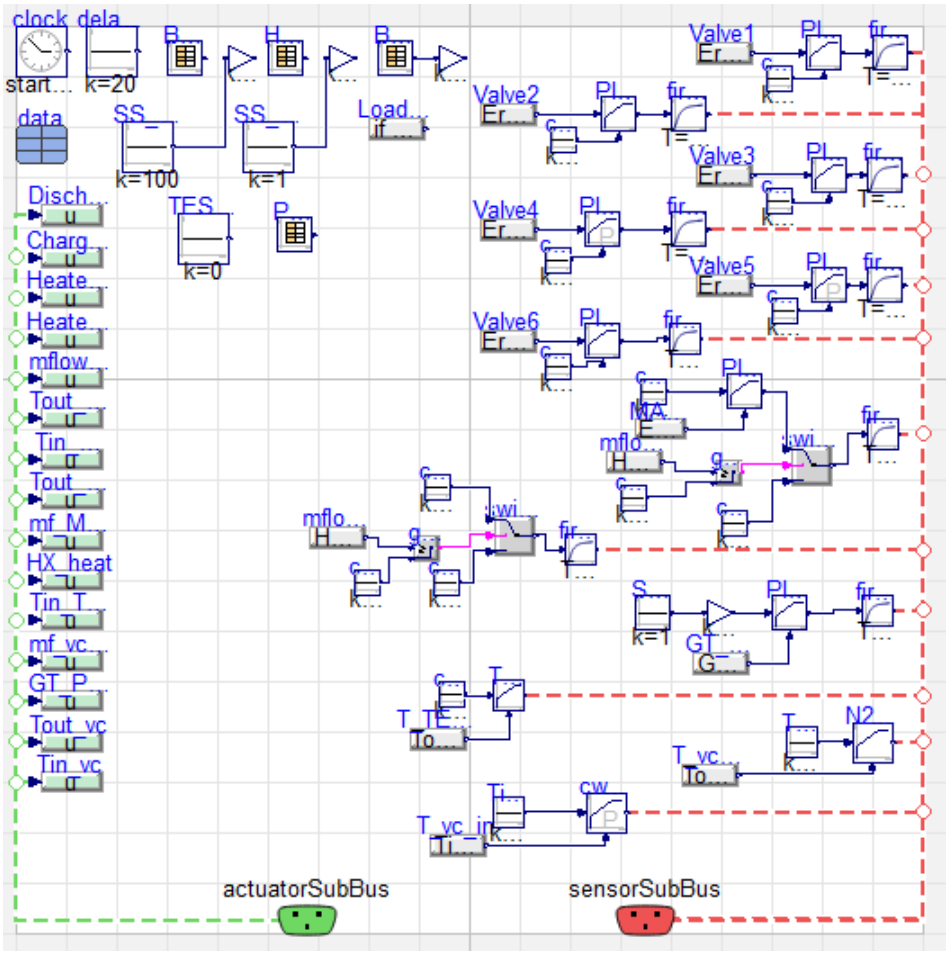

Figure 11. Central control scheme values specified in the operational modes.

The benefit of integrating MAGNET with TEDS and a PCU is seen in the resulting dispatch flexibility. In response to market conditions, thermal energy can be directed to electricity production, heating demand, thermal storage, or any combination of the three. The thermal storage can also discharge to the heat load when necessary. The increased flexibility of the system comes at the price of increased complexity of the controls. To control all the hybrid system's subsystems and components, a single centralized control system must be developed to cover all its potential operating modes. The operating modes are listed in Table 2 below.

Table 2. Foreseeable operating modes.

Mode	Heat Source to Electricity Load	Heat Source to Heat Load	Heat Source to Storage	Storage to Heat Load
1	Yes	Yes	No	No
2	Yes	No	Yes	No
3	Yes	Yes	Yes	No
4	Yes	Yes	No	Yes

Note that this operating scheme assumes that the PCU is always running and is always needed to meet the electricity load. Thus, in all the operating modes, the heat source will be directed to meet the electricity load, as shown in Table 3. A more complex operating scheme will eventually be developed to accommodate scenarios in which there is no electricity demand, with the heat source instead directing all its energy toward the heat load and/or thermal storage.

In Mode 1, the hybrid system operates in a standard operating mode in which all the thermal energy produced by the heat-generation source (i.e., MAGNET) is distributed to meet the demand of the electricity and heat loads. Note that in this control scheme, the electricity demand is most highly prioritized, thus the thermal energy is first distributed to meet this demand, then the excess thermal heat can be distributed to the heat load. The thermal storage is not in use, as neither charging nor discharging occurs in this mode.

In Mode 2, the hybrid system simulates a charging mode in which the thermal generator, after meeting the electricity demand, sends all excess energy to the thermal storage. As there is no heat load, the thermal storage does not discharge.

In Mode 3, which is a combination of Modes 1 and 2, the hybrid system—after meeting the electricity demand—distributes the excess heat to TEDS so it can be discharged to the heat load. However, because the heat load is less than the amount of heat distributed to TEDS, the remainder of the excess heat is stored inside the thermocline storage.

Mode 4 utilizes both the heat-generation source and the thermal storage to meet the heat demand. This operating mode is used when the heat demand exceeds the amount of excess heat provided by MAGNET. The thermocline storage will discharge its stored thermal energy to help meet this unmet heat demand.

To ensure proper dispatch of thermal energy, a combination of nine valves is used to regulate the flow rate of the coolant through the proper channels. These valves are illustrated in Figure 10. The valves and their control will be explained in Section 3.1.3.2.

Table 3. Valve positions to direct the DETAIL system to meet various operation mode conditions.

Valve	Position (Mode 1)	Position (Mode 2)	Position (Mode 3)	Position (Mode 4)
1	Closed	Open	Open	Close
2	Open	Closed	Open	Open
3	Closed	Closed	Closed	Open
4	Closed	Open	Open	Closed
5	Closed	Closed	Closed	Open
6	Open	Open	Open	Open
7	Open	Open	Open	Open
8	Open	Open	Open	Open
9	Open	Open	Open	Open

3.1.3.1 Supervisory Control Scheme

While it is possible to input individual demand signals for each component of the hybrid system, it is imperative that the hybrid system take in market demand scenarios and make control decisions based on these market demands. Therefore, the supervisory control scheme is designed to make dispatch decisions based solely on two separate market demand inputs: electricity demand and heat demand. Electricity

demands will be met by the PCU, and the heat demand will be met by the excess thermal energy from MAGNET. Energy systems integrated with some form of storage typically use an objective function to maximize profitability if operated in a market system, or to meet an overall demand if operated within a microgrid—with the IES being meant to meet all the energy needs of the microgrid. In either scenario, it is most advantageous for the heat-source generator to operate at maximum capacity, especially if the heat-source generator is a nuclear reactor. During times of low prices/demand, the excess heat can be stored through a bypass valve. This stored energy can then be discharged during times of high prices/demand.

In this simulation, the control scheme is designed to meet the overall demand of the grid, both electrical and thermal, with any excess thermal energy being dispatched to and stored within the thermocline thermal storage. As the electricity demand can oscillate in respect to time, the amount of excess heat redirected to TEDS will also vary. To determine the amount of heat sent to TEDS after meeting the electricity demand, the amount of heat provided via the helical coil heat exchanger between MAGNET and TEDS is used as an input to the supervisory control scheme. The TES demand can then be calculated by applying the heat amount and heat demand input as follows:

$$Load_{TES}(t) = Heat_{HX}(t) - Heat_{demand}(t) \tag{7}$$

where $Load_{TES}$ is the TES demand, $Heat_{HX}$ is the amount of heat being provided by the MAGNET-TEDS heat exchanger, and $Heat_{demand}$ is the heat demand of the microgrid. If $Load_{TES}(t) > 0$, the excess thermal energy will be stored in the thermocline. If $Load_{TES}(t) < 0$, the thermal storage unit will begin to discharge.

3.1.3.2 Control Strategies

To ensure proper dispatch of heat within the integrated system, the supervisory control system requires input from external variables (market demands) and internal variables (the mass, temperature, and flow rate inside the system). This is achieved through different sensors located inside the loop, as shown in Figure 10. These sensors communicate to the centralized control unit the current state at various points in the system, based on which, decisions can be made to achieve the overall objective of the integrated system. All controllers in the system are PI controllers instead of a proportional integral derivative (PID) or proportional controllers.

Valve 1: Valve 1 is a globe valve inside TEDS and was designed to regulate the Therminol-66 flow to meet a charging flow-rate setpoint, using flow meter-202 (FM_{202}):

$$\dot{m}_{chargingDemand} = \frac{Load_{TES}}{C_{pavg}(T_{HotSP} - T_{ColdSP})} \; if \; Load_{TES} > 0, else \; 0 \tag{8}$$

$$Error_1 = \frac{\dot{m}_{chargingDemand} - FM_{202}}{\dot{m}_{chargingMax}} \tag{9}$$

Valve 2: Valve 2 is a globe valve inside TEDS and was designed to regulate the flow to meet the heat demand. This valve is controlled via referred signals from FM_{003} and FM_{202}:

$$\dot{m}_{HeatDemand} = \frac{Heat_{demand}}{C_{pavg}(T_{HotSP} - T_{ColdSP})} \tag{10}$$

$$Error_2 = \frac{\dot{m}_{HeatDemand} - (FM_{003} - FM_{202})}{\dot{m}_{HeatMax}} \tag{11}$$

Valve 3: Valve 3 is a globe valve inside TEDS and was designed to regulate the flow to meet the discharging flow-rate set point, using FM_{201}:

$$\dot{m}_{dischargingDemand} = \frac{|Load_{TES}|}{C_{pavg}(T_{HotSP} - T_{ColdSP})} \; if \; Load_{TES} < 0, else \; 0 \tag{12}$$

$$Error_3 = \frac{\dot{m}_{dischargingDemand} - FM_{201}}{\dot{m}_{dischargingMax}} \tag{13}$$

Valve 4: Valve 4 is a ball valve inside TEDS and was designed as part of an interlocking system that includes Valve 1, with a 5-second opening delay to ensure that the charging and discharging lines are not open simultaneously. If the charging demand is zero, Valve 4 will close to ensure that the charging line is closed. If the charging demand is above zero, Valve 4 will wait 5 seconds to allow the discharge line to fully close before it moves to a fully open position.

Valve 5: Valve 5 is a global valve that works within an interlocking system that includes Valve 3. This system was designed in the same manner as the interlocking system encompassing Valves 1 and 4, only this time for the discharging line. When the discharge demand exceeds zero, Valve 3 will start to open, while Valve 5 will wait an additional 5 seconds before opening in order to ensure that the charging line is closed while the discharging mode is in operation.

Valve 6: Valve 6 is a global valve in TEDS, and it regulates the flow from the thermocline to the MAGNET-TEDS heat exchanger. It was designed to open whenever excess thermal energy from MAGNET needs to be stored.

Valve 7: Valve 7 is a global valve connecting MAGNET and the PCU. It was designed to regulate the flow rate from MAGNET so as to meet the electricity demand from the market. The opening of Valve 7 oscillates until the PCU power output matches the electricity demand input from the market. The exact amount of flow rate needed to meet the electricity demand can be calculated based on the relationship between the flow rate and the electricity produced, as described in Section 3.1.1.

Vale 8: Valve 8 is a global valve connecting MAGNET and TEDS. It directs the excess hot coolant from MAGNET to TEDS by using the following flow meters: $FM_{MAGNET-TEDS}$, FM_{MAGNET}, and $FM_{MAGNET-PCU}$. This is illustrated in the equations below:

$$\dot{m}_{MAGNET-TEDS} = FM_{MAGNET} - FM_{MAGNET-PCU} \tag{14}$$

$$Error_{MAGNET-TEDS} = \dot{m}_{MAGNET-TEDS} - FM_{MAGNET-TEDS} \tag{15}$$

where $\dot{m}_{MAGNET-TEDS}$ is the flow rate between MAGNET and TEDS, $\dot{m}_{MAGNET-TEDS}$ is the flow rate inside the MAGNET loop, and $\dot{m}_{MAGNET-PCU}$ is the flow rate between MAGNET and the PCU.

Valve 9: Valve 9 is a ball valve that interlocks with Valve 8, and also features a 5-second delay. This interlocking system works in the same way as those of Valve 1 and Valve 4, and Valve 3 and Valve 5. When excess thermal energy must be redirected to TEDS, Valve 8 opens, followed by Valve 9 exactly 5 seconds later. When there is no excess energy to redirect, Valve 8 closes, followed by Valve 9 exactly 5 seconds later.

Pump: A PI controller is implemented to control the flow inside TEDS by regulating the discharge pressure of the pump. To maintain the inlet temperature of TEDS at its design charging temperature (325°C), the flow rate must change when the temperature changes. Temperature changes occur due to changes in heat being discharged from MAGNET. Using the heat rate from MAGNET, the nominal mass flow rate can be calculated via Equation 16, and the heat deposited into TEDS from MAGNET can be calculated via Equation 17.

$$\dot{m}_{TEDS} = \frac{Q_{MAGNET-TEDS}}{C_{pavg}(T_{HotSP} - T_{ColdSP})} \tag{16}$$

where $\dot{m}_{TEDS}$ is the flow rate of Therminol®-66 inside TEDS and $Q_{MAGNET-TEDS}$ is the amount of heat transferred between MAGNET and TEDS. Using the following equation, the control algorithm calculates the amount of heat being transferred via the heat exchanger:

$$Q_{MAGNET-TEDS} = \dot{m}_{MAGNET-TEDS} \begin{bmatrix} H_{moderator}\left(p_{MAGNET_{in}}, T_{MAGNET_{in}}\right) \\ -H_{moderator}\left(p_{MAGNET_{out}}, T_{MAGNET_{out}}\right) \end{bmatrix} \quad (17)$$

where $Q_{MAGNET-TEDS}$ is the heat transferred from MAGNET to TEDS. This value is dependent on the coolant flow rate through the heat exchanger ($m_{flow_{MAGNET_{TEDS}}}$), the inlet ($p_{MAGNET_{in}}$) and outlet pressure ($p_{MAGNET_{out}}$) of the coolant, and its respective temperatures ($T_{MAGNET_{in}}, T_{MAGNET_{out}}$).

Chiller: The discharged Therminol®-66 transfers thermal heat through the ethylene glycol chiller. The ethylene glycol flow rate is moderated in modeling to maintain the exit temperature of Therminol®-66 at its cold design temperature (225°C). This is accomplished using the signal from temperature sensor TC_{005}:

$$Error_{chiller} = TC_{005} - T_{ColdSP} \quad (18)$$

If the exit temperature is lower than the cold set point, the glycol flow rate would decrease, reducing the amount of heat transferred from the Therminol®-66 and thus increasing the exit temperature of the oil. If the exit temperature is higher than the cold set point, the glycol flow rate would increase, causing more heat to be transferred across the tubes and thus raising the exit temperature. Furthermore, to prevent the ethylene glycol from boiling, a minimum flow rate constraint is imposed on the chiller flow rate. This means that, during times of low discharged Therminol®-66 temperatures (potentially when the storage has not been sufficiently charged) or low Therminol®-66 flow rates, the exit temperature may drop below the cold set point. This constraint is needed to ensure that the ethylene glycol does not boil, thereby fouling the heat exchanger.

In addition to these valves, pump, and chiller controllers, other PI controllers are used to regulate the flow inside MAGNET (see Section 2.1.3). A summary of each controller's measured quantity, reference value, gain, and controlled element is given below in Table 4.

Table 4. Summary of PI controllers used in the integrated system.

Controller	Measured Quantity	Reference Value	Gain	Controlled Element
1	$Error_1$	0	0.126	Valve 1
2	$Error_2$	0	2.52	Valve 2
3	$Error_3$	0	0.756	Valve 3
4	$Error_4$	0	25.2	Valve 4
5	$Error_5$	0	25.2	Valve 5
6	$Error_6$	0	25.2	Valve 6
7	$Error_{MAGNET-TEDS}$	0	-0.252	Valve 8
8			On/Off	Valve 9
9	W_{PCU}	GT_{demand}	0.00007	Valve 7
10	$T_{TEDS,charged}$	T_{hotSP}	-0.125	TEDS pump
11	$T_{vc,out}$	602°C	-0.00025	$m_{flow_{MAGNET}}$
12	$T_{vc,in}$	363°C	-0.001	Chilled water flow rate
13	$T_{TEDS,discharged}$	T_{ColdSP}	-1	Ethylene glycol flow rate

3.2 Simulation

This section gives the simulation results for the integrated system in all four operating modes. The capability of the integrated system to handle transient operational modes is discussed, along with its performance. A shakedown testing scenario was created to evaluate the technical performance and integration of all the subsystems and components, as well as how they all work together under one centralized control unit.

3.2.1 Shakedown Testing

To demonstrate the different operating modes of the integrated system, a test case was built to illustrate the operation of all four modes. The results are shown in Figure 12, with the different modes being color-coordinated (see Table 5) for clarity.

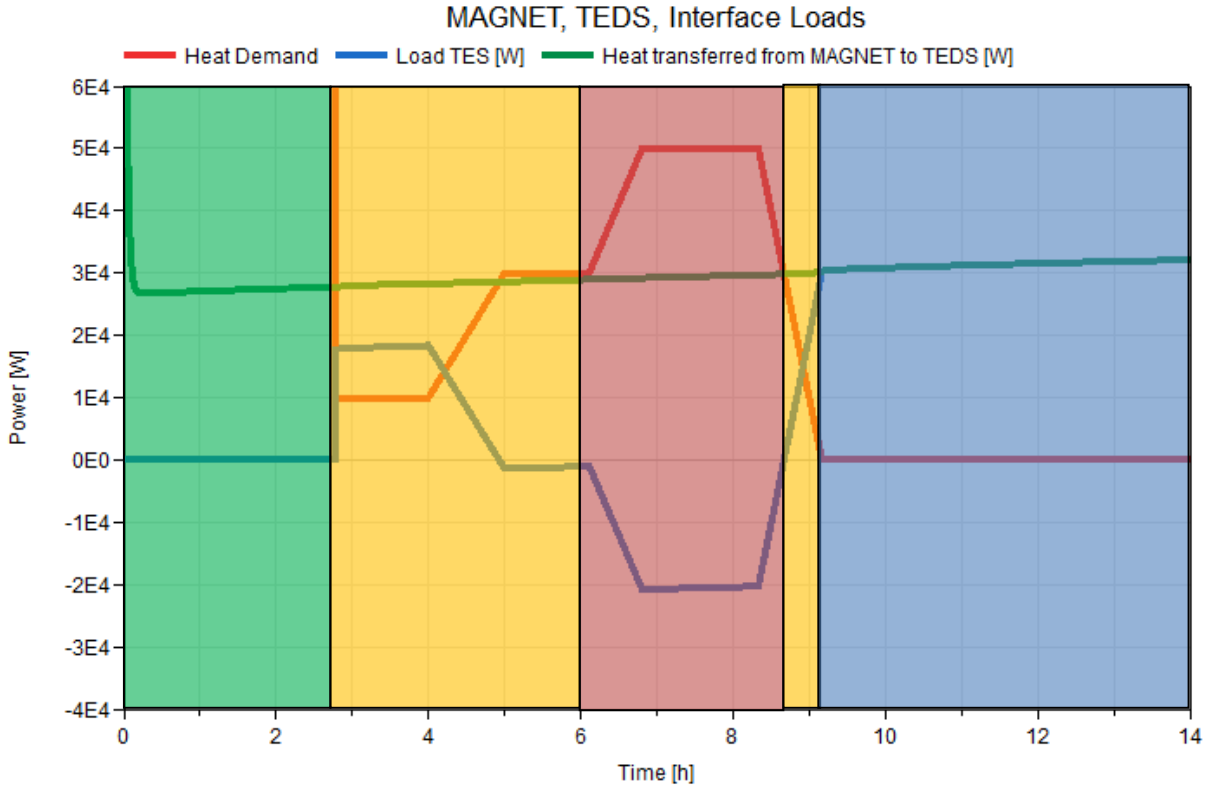

Figure 12. Heat transferred from MAGNET to TEDS, the heat demand, and the storage load. The colors green, blue, yellow, and red correspond to the modes 1, 2, 3 and 4, respectively.

The thermal storage was simulated as being complete empty at the start of the simulation, with every node inside the thermal storage being set to 225°C. During the first 10,000 seconds (i.e., 2.8 hours), the integrated system operated in Mode 1, with the thermal energy being used to meet the electrical demand first, and all excess energy being used to meet the heat demand in TEDS. Valve 2 was open to allow the heat from MAGNET to flow straight to the ethylene glycol heat exchanger in order to meet the heat demand imposed on the system. As shown in Figure 12, the TES load was at 0 during this time period, and the heat demand was equal to the amount of heat transferred from MAGNET to TEDS. No storage charging or discharging occurred during this time, meaning that Valves 1, 3, 4, and 5 were closed. This was done to allow sufficient simulation time for initialization. This initiation process can be seen in Figure 13 and Figure 14, where the flow rate inside the integrated system fluctuates to reach the optimal solution.

After the first 10,000 seconds, the integrated system shifts into Mode 3. This is signaled by the decrease in the heat demand on the system. As shown in Figure 12, the heat demand dropped lower than the amount of heat available from the MAGNET loop, causing the thermocline storage to begin its charging operation. This was accomplished by opening Valves 1 and 4 to align with the charging operational mode. Valves 3 and 5 remained closed to prevent the thermal storage from discharging. However, the heat demand was not completely zero, as some of the excess heat from MAGNET was still directed to the ethylene glycol heat exchanger to meet the heat demand. As shown in Figure 14 and Figure 15, the necessary flow rate was successfully regulated to meet both the heat and charging demands.

This was done even as the heat demand started rising again at hour 4, with Mode 4 not being shifted to until hour 6. As the heat demand continued to rise, it eventually surpassed the amount of heat available from MAGNET. Thus, the thermal storage began to discharge, as shown in Figure 12 and Figure 14. With the heat demand flow rate exceeding the flow rate available from MAGNET, the thermal storage was able to meet the required discharge flow rate. The heat demand started to fall, as did the discharging flow rate, until the heat demand matched the amount of heat being dispatched from MAGNET.

At around 8.5 hours, this heat demand also dropped below the maximum amount of heat available from MAGNET. Thus, Mode 3 was again switched to, charging the thermal storage by using the excess heat not needed to meet the heat demand of the system. Eventually, the heat demand fell to zero, and all the heat available from MAGNET was then dispatched to the thermocline storage, causing a switch to Mode 2.

The exit temperature of the vacuum chamber inside the MAGNET loop was successfully kept constant at 600°C—as shown by the blue line in Figure 13—by modulating the flow rate within MAGNET. The TEDS loop inlet temperature was also successfully kept at 325°C after the initiation process during the first 10,000 seconds, as shown by the green line in that same figure.

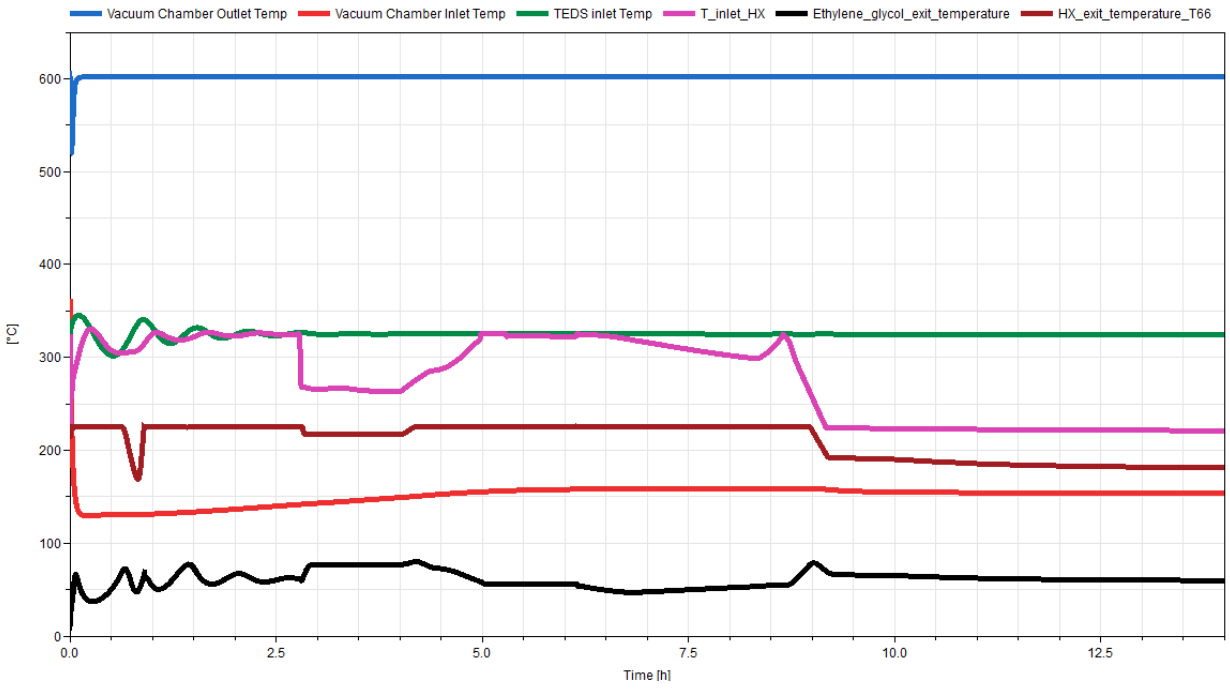

Figure 13. Temperatures calculated throughout the MAGNET-TEDS-PCU integrated system.

The Therminol®-66 ’s exit temperature from the ethylene glycol heat exchanger slightly decreased to 220°C after the first 10,000 seconds, as the thermal storage began to charge. This was due to the decrease

in the Therminol®-66 ’s temperature at the heat exchanger inlet, as shown in magenta in Figure 13. Due to the minimum flow rate constraint of the ethylene glycol fluid in the heat exchanger, the exit temperature of the Therminol®-66 dropped. The decrease in the inlet temperature was caused by the partial charge operation in Mode 3, during which some of the heated Therminol®-66 was routed to the thermocline for charging. As the heated fluid entered the top of the thermocline tank, the cold fluid at the bottom of the tank was discharged. Since no charging operation occurred during the initial 10,000 seconds, the fluid inside the thermocline tank began to decrease in temperature, as shown in Figure 16. As the heat demand started to increase, the charging decreased, leading to a rise in the inlet and outlet temperatures. These temperatures started to decrease again during the full-charging operation mode at the end of the simulation, as shown in Figure 13. During the discharge operation, the inlet temperature started to slightly decrease as the hot fluid was discharged, but since the thermocline was not sufficiently charged, the temperature at the top of the tank began to decrease as well, as seen in Figure 16. The inlet temperature briefly rose again when the discharge stopped. Finally, at the end of the simulation, with the system being in full charging mode, the Therminol®-66 inlet and exit temperatures for the ethylene glycol heat exchanger again dropped.

The ethylene glycol temperature also fluctuated during the initiation process at the beginning of the simulation. As the temperature of the Therminol®-66 entering the heat exchanger dropped, the ethylene glycol flow rate fell to its minimum set flow rate to prevent the ethylene glycol from boiling. As shown in Figure 13, the ethylene glycol temperature never exceeds 100°C.

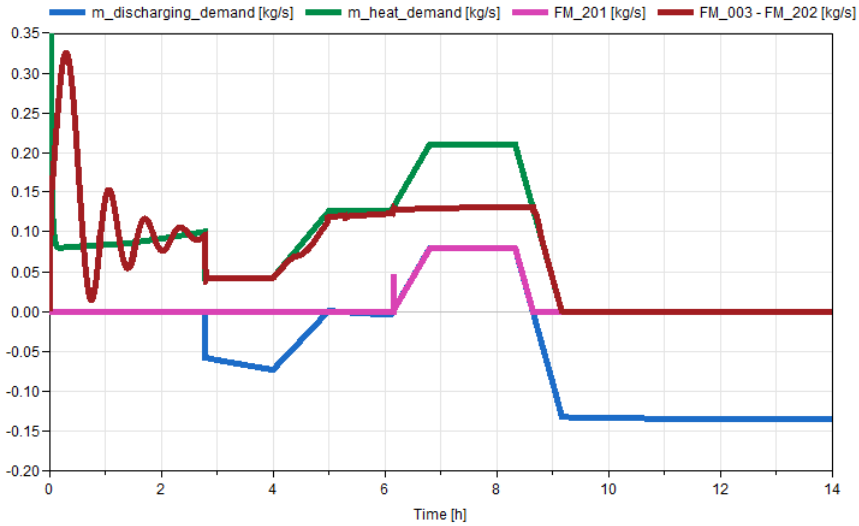

Figure 14. Discharging demand flow rate and heat demand flow rate.

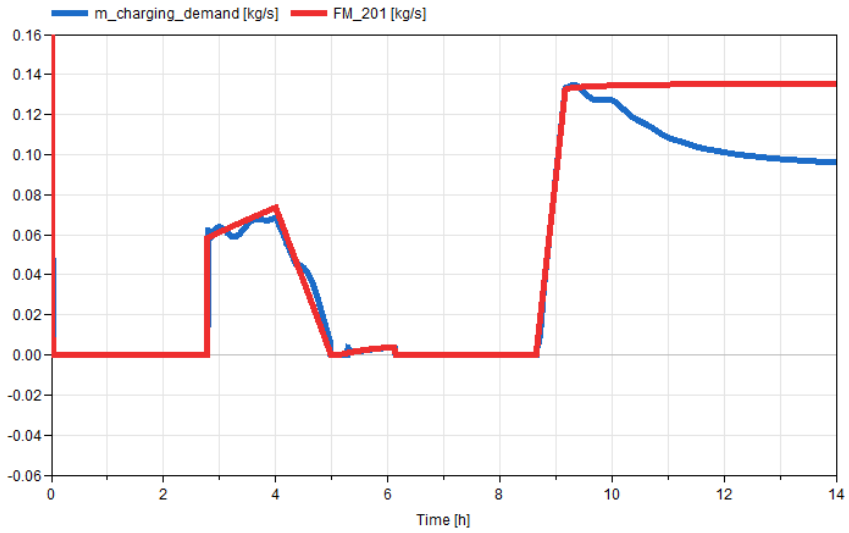

Figure 15. Charging demand flow rate.

Figure 16 shows the temperature at various locations inside the thermocline storage tank: at the top of the tank; 25%, 50%, and 75% of the way down the tank; and at the very bottom of the tank. The thermocline was initially set to be fully discharged. It was bypassed during the first 10,000 seconds of the simulation, as all the heat from MAGNET was sent to meet the heat demand of the integrated system. As a result, the temperature inside the thermocline started to drop as heat was lost to the surrounding environment. At 10,000 seconds, the storage tank started to charge; thus, the temperature at the top of the tank started to rise, leveling at about 320°C after the charging decreased. At 6 hours, the temperature at the top began to decrease, as the tank was then in discharging mode. When the tank entered charging mode again at about 9 hours, the temperature again started to increase. At the end of the 14 hours, the tank was almost 25% charged.

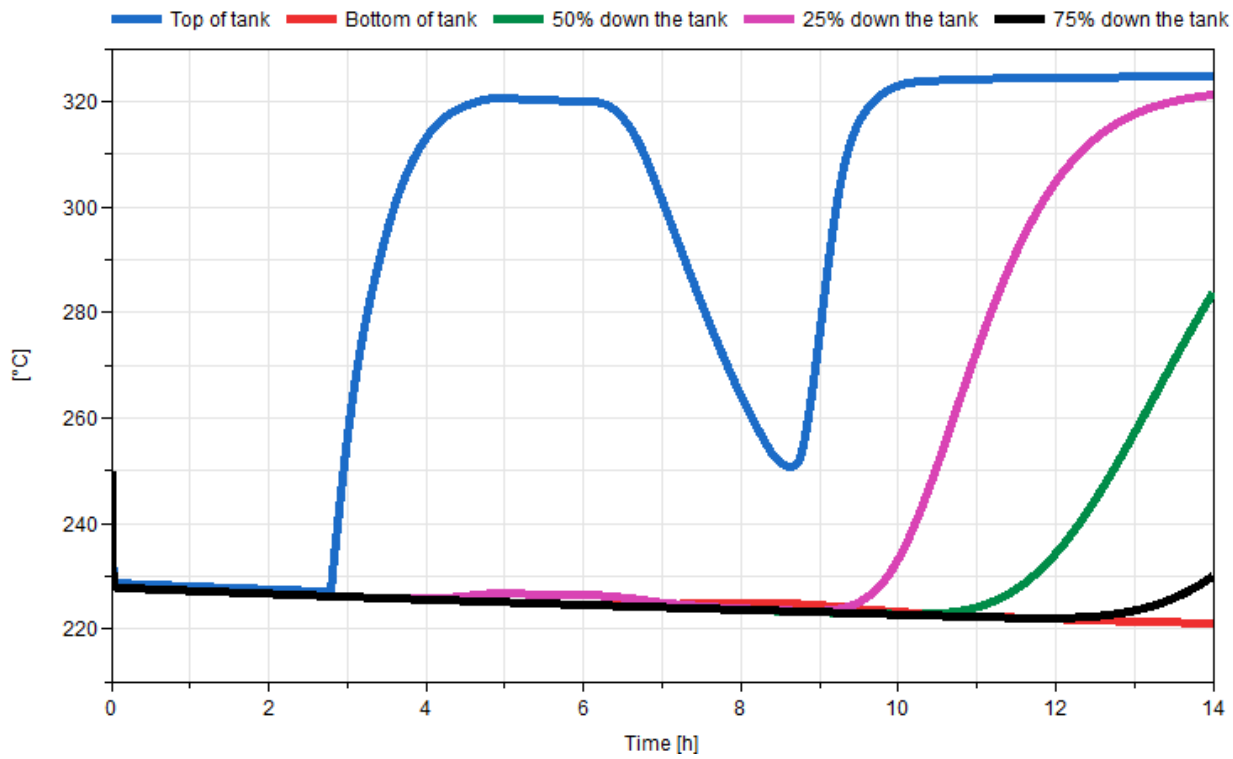

Figure 16. Temperature of the thermocline fluid at various locations within the tank.

4. HIGH-TEMPERATURE STEAM ELECTROLYSIS

HTSE is a water electrolysis process—occurring at temperatures of 700–1000°C—in which electrical energy is the driving force for splitting water/steam to produce oxygen and hydrogen, using solid oxide cells. Compared to other hydrogen production processes such as proton-exchange membrane and high-temperature thermochemical processes, HTSE offers several advantages, including no greenhouse gas production, consumption of non-fossil fuel sources, high efficiency thanks to lower voltage and current losses (which further decrease with increases in temperature), and a less corrosive environment at high temperatures [8].

Figure 17 shows a schematic of a HTSE cell, which consists of a cathode, an electrode, and an anode stacked on top of each other. A mixture of steam and hydrogen is fed to the cathode side, where the steam, when in the presence of a catalyst and electric current, splits into hydrogen and oxygen. The steam-hydrogen mixture fed to the cathode is about 90%-10% (mole fraction) so as to maintain a hydrogen-reducing atmosphere on the HTSE cells in order to slow the rate of cell degradation. The hydrogen needed for this mixture composition is initially provided by an external source, but is recycled from the outlet stream once the HTSE system is running. The electrolyte allows the oxygen to pass through it to the anode side, where it is swept by a sweep gas such as air. Several cells are combined to form a stack in order to meet the necessary capacity or hydrogen production rate.

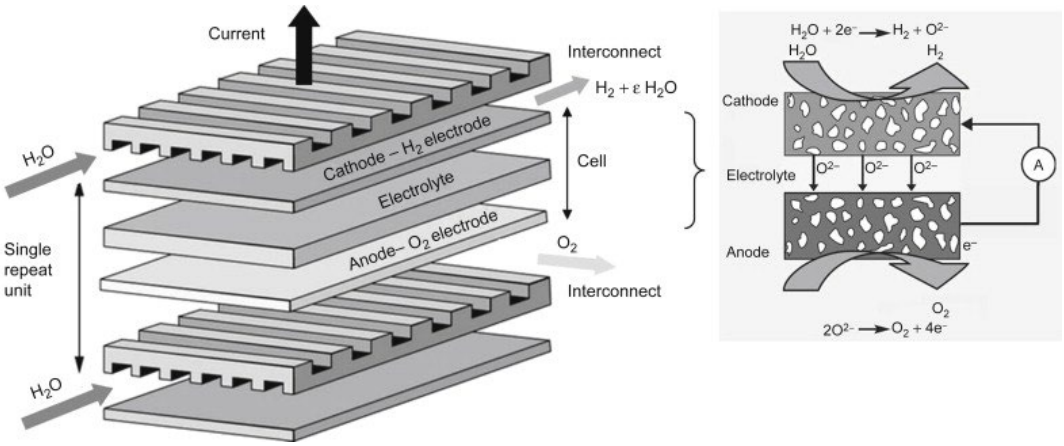

Figure 17. Schematic of a high-temperature steam electrolysis cell [9].

Several HTSE stacks are currently being performance-tested at INL's Energy Systems Laboratory. These vary in desgn, operations, as well as rating. One such system is a 30 kW reversible solid oxide cell, which can be run in both electrolysis and fuel cell mode. During electrolysis, the system consumes steam and electricity to produce hydrogen, whereas in the fuel cell mode it consumes hydrogen to produce electricity and water. In this study, only the electrolysis mode is described.

4.1 Model Development

The HTSE model can be broken down into individual components (i.e., the SOEC, the recuperative heat exchangers, a condenser, and a recycler). The SOEC is the main component, as the splitting of steam into hydrogen and oxygen takes place inside it, whereas the other components allow for heat transfer between the inlet and outlet stream, as well as maintain the inlet stream composition. The following sections describe each of the components in detail.

4.1.1 Solid Oxide Electrolysis Cell Modeling

The SOEC model was initially developed as a design problem that matched the operating conditions of the HTSE setup in the Energy Systems Laboratory, as the actual design is proprietary. The design and operation conditions used to set up the model are provided in Table 6.

Table 5. Design and operating conditions of the HTSE stack.

Parameter	Value
System operating pressure (bar)	1.013
System operating temperature (°C)	790
Power Input (kWe - DC)	30
Operating voltage (V)	1.283
Active cell area (cm^2)	110.8
Area specific resistance (Ω/cm^2)	1.3

To calculate the open circuit voltage (OCV) of the cell being used for the analysis, the cell potential and Nernst contribution had to be calculated. The standard cell potential is calculated by knowing the Gibbs free energy of reaction. To acquire this, the following methodology was followed.

For steam electrolysis, the stoichiometric equation is as follows, and was used to set up the Gibbs free energy equation:

$$H_2O \rightarrow H_2 + \frac{1}{2} O_2 \tag{19}$$

The Gibbs free energy of reaction is the difference between the Gibbs free energy of formation of the products and that of the reactants:

$$\Delta G^{\circ} = \sum(\Delta G_f)_{products} - \sum(\Delta G_f)_{reactants} \tag{20}$$

To calculate the Gibbs free energy for the reactants and the products, the following 7-term polynomial was derived:

$$\frac{G_T^{\circ}}{RT} = \frac{H_T^{\circ}}{RT} - \frac{S_T^{\circ}}{R} = a_1[1 - \ln(\mathrm{T})] - \frac{a_2 T}{2} - \frac{a_3 T^2}{6} - \frac{a_4 T^3}{12} - \frac{a_5 T^4}{20} - \frac{a_6}{T} - a_7 \tag{21}$$

where a_1–a_7 represent the polynomial terms for the Gibbs free energy equation and can be found in [10] and T is the operating temperature of the cell. The standard cell potential is then calculated per:

$$\Delta G_{cell}^{\circ} = -nFE_{cell}^{\circ} \tag{22}$$

where n represents the number of electrons transferred and F is Faraday's constant. Furthermore, the Nernst potential is calculated based on the partial pressures of the reactant and products:

$$EE = E^{\circ} + \frac{RT}{nF} ln \frac{[p_{reactants}]}{[p_{products}]} \tag{23}$$

The OCV is then calculated by adding together the cell potential and the Nernst potential. The current density of the cell is calculated using the cell operating voltage, the OCV, and the area-specific resistance:

$$Current\ Density = \left| \frac{Operating\ Voltage - OCV}{ASR} \right| \tag{24}$$

The cell current is then calculated by multiplying the current density by the cell area. This cell current is multiplied by the total number of cells, and is used to calculate the number of moles of hydrogen produced. Based on the cathodic reaction shown below, two electrons are consumed to produce 1 mole of hydrogen:

$$H_2O + 2e^- \rightarrow H_2 + O^{2-} \tag{25}$$

This also enables calculation of the oxygen moles produced by splitting the steam molecule. From the above equation, it is evident that for 1 mole of hydrogen produced, so is half a mole of oxygen. This oxygen ion transfers from the cathode side, through the electrolyte, and to the anode side, where it is swept by the sweep gas. As the sweep gas used in this model is air, the stream leaving the anode is oxygen-rich air.

To account for the energy flow caused by the splitting of water, the production of hydrogen and oxygen, and the transfer of energy to the anode side, the energy transfer equations are appropriately included within the SOEC model. The base SOEC model is shown below in Figure 18.

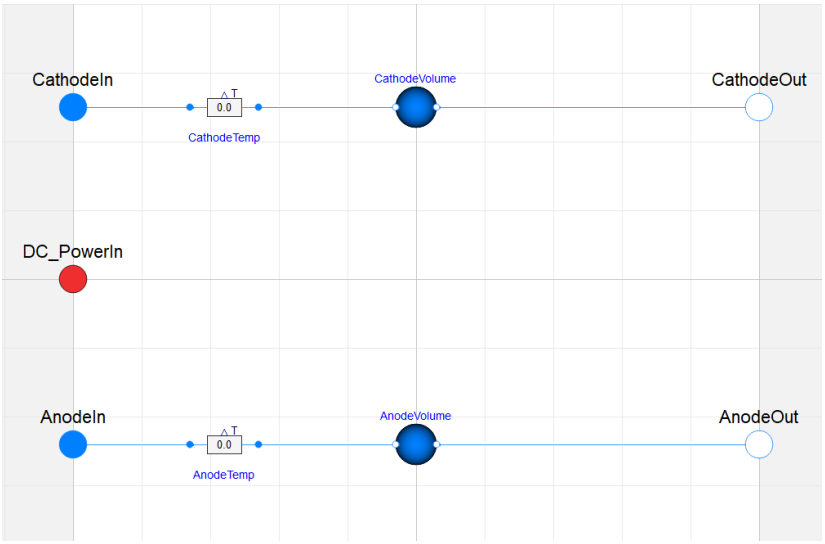

Figure 18. SOEC base model.

Once the base SOEC model was developed, it was coupled with flow boundary conditions to test the steam utilization and compare the results to an equivalent steady-state model developed in Aspen HYSYS. Figure 19 shows the Dymola-based SOEC model, and Table 7 compares the values from the developed SOEC model and the Aspen HYSYS model.

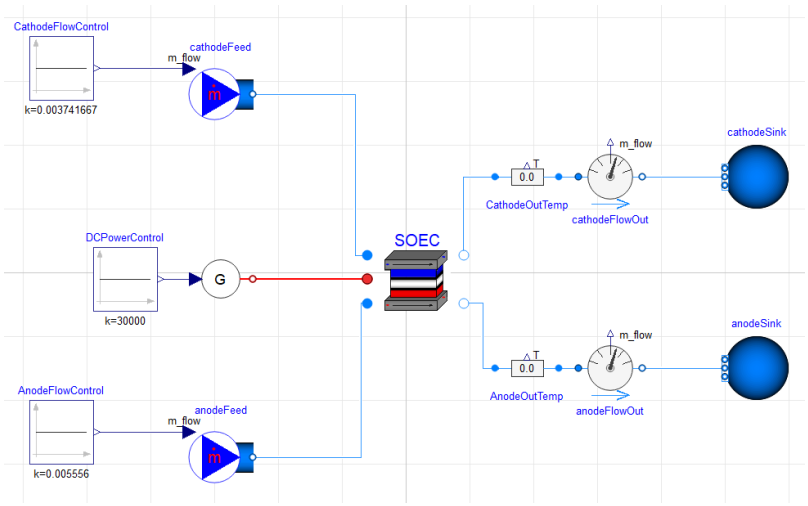

Figure 19. Dymola-based model of a standalone SOEC.

Table 6. Comparison between the Dymola and Aspen HYSYS models.

Parameter	Dymola	Aspen HYSYS	% Difference
Steam utilization	59.8	60	0.33
Hydrogen produced (mol/s)	0.1212	0.123	1.46
Oxygen transferred (mol/s)	0.06058	0.06097	0.64
Total hydrogen produced (kg/h)	1.045	1.058	1.23

It is evident that both the Dymola and Aspen HYSYS models agree well with each other. The minor percent differences between the two models could be attributed to rounding errors, as well as to fluid property differences stemming from the fluid packages used within the individual software.

4.1.2 High-Temperature Steam Electrolysis Modeling

Once the SOEC model was developed, additional components were incorporated to develop the HTSE system. This included the addition of recuperative heat exchangers, trim heaters, a condenser, and a recycler. Figure 20 shows a schematic of the Dymola-based model for the HTSE system. The heat exchangers used in this model were chosen from the TRANSFORM library and were sized using data acquired from an equivalent Aspen HYSYS model. The trim heaters were modeled as simple volumes, the heat input to which was adjusted to ensure an exit temperature of 790°C. This heat input was adjusted using a PID controller. The details of the condenser and recycler are provided in the following sections.

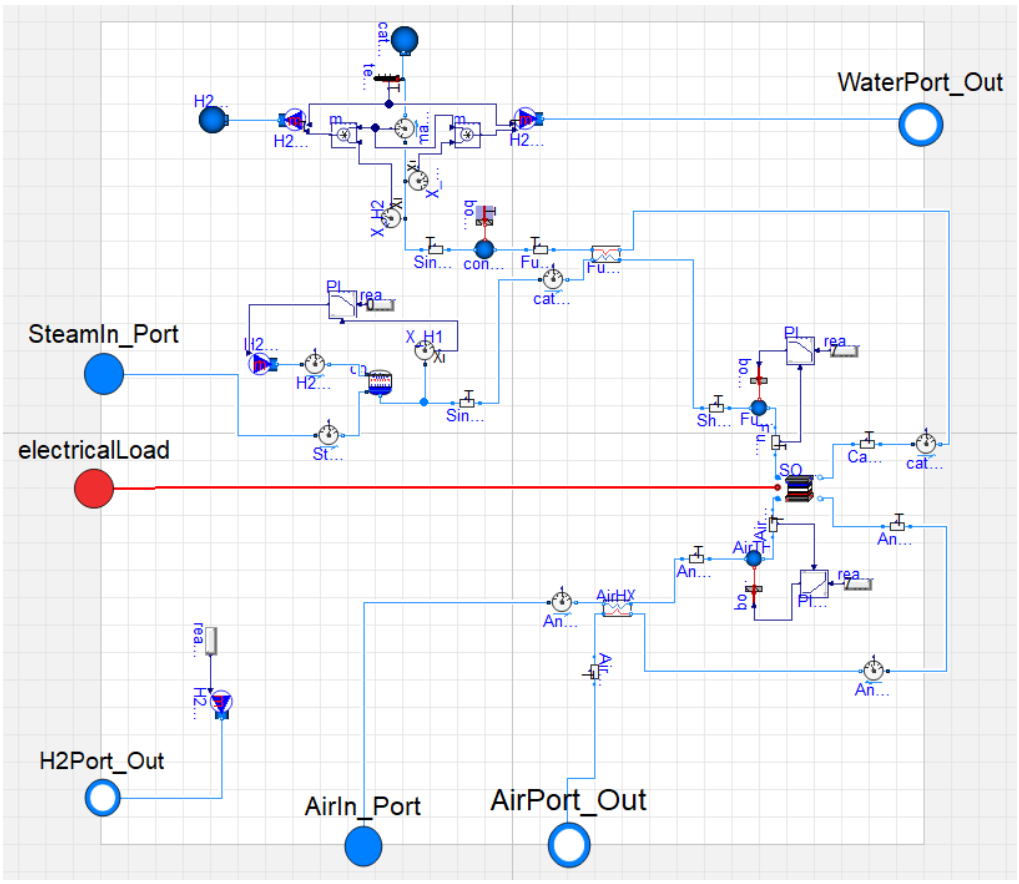

Figure 20. Components within the HTSE model.

4.1.2.1 Condenser

The condenser in the HTSE model allows for condensation of the steam and the cooling of hydrogen from the product stream. However, as modeling a heat exchanger with a multispecies stream in which one stream condenses and the other cools proved a challenging effort, a simplification was made to allow for a component splitter to ideally separate the hydrogen and steam and allow them both to cool to 40°C. Figure 21 shows a schematic of an ideal component splitter. This model measures the mass fractional flow and temperature of individual species within the incoming stream and provides that information to two separate mass flow sources. The mass flow sources then produce a flow of that pure species at the measured temperature and provide it to outlet boundary ports. The incoming flow is then sent to a sink.

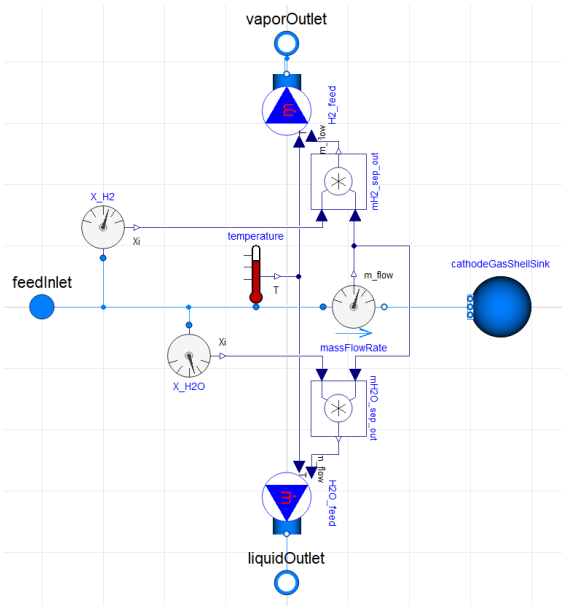

Figure 21. Dymola-based model of an ideal component splitter.

The HTSE model includes a cooler that cools the stream going into the component splitter. The boundary ports from the component splitter provide the outlet flow of condensed water and cooled hydrogen produced from the HTSE system.

4.1.2.2 Hydrogen Recycler

To maintain a reducing environment on the cathode side of the SOEC, 10% of the gas stream fed to it must be hydrogen. To ensure this, some of the produced hydrogen is recycled back into the system and run through the SOEC. This is achieved through a hydrogen recycle component that consists of a hydrogen mass flow source, mass flow-rate sensors, a PID controller, and an ideal combiner. Figure 22 shows a schematic of the recycler used in the HTSE model.

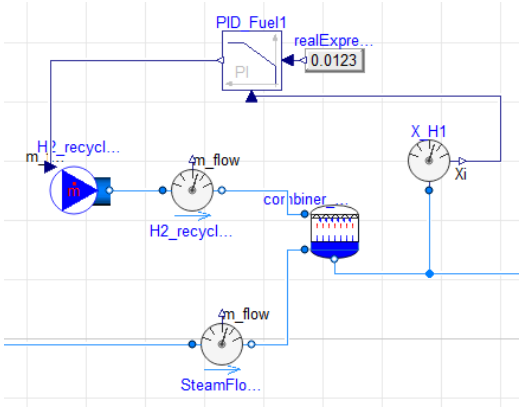

Figure 22. Dymola-based model of a recycler.

By measuring the composition of the stream exiting the combiner, the PID controller dictates the flow of the hydrogen mass flow source in order to maintain a 90%-H2O/10%-H2 molar fraction in the stream. The combiner operates in a fashion similar to the component splitter; however, instead of splitting, it mixes the incoming streams. Figure 23 shows a schematic of an ideal fluid combiner. In the HTSE model, this component mixes the steam and hydrogen streams.

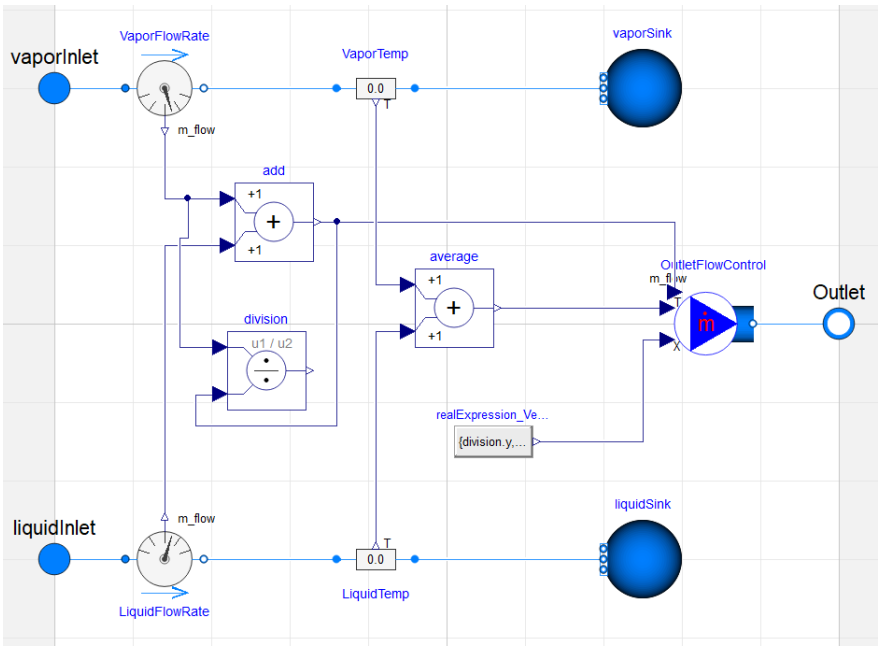

Figure 23. Dymola-based model of an ideal fluid combiner.

Once the components are connected to appropriate fluid ports, fluid boundary sources and sinks—as well as a DC power source—are connected to the HTSE model. The completed HTSE model is shown in Figure 24. The results acquired from the model are presented in the following section.

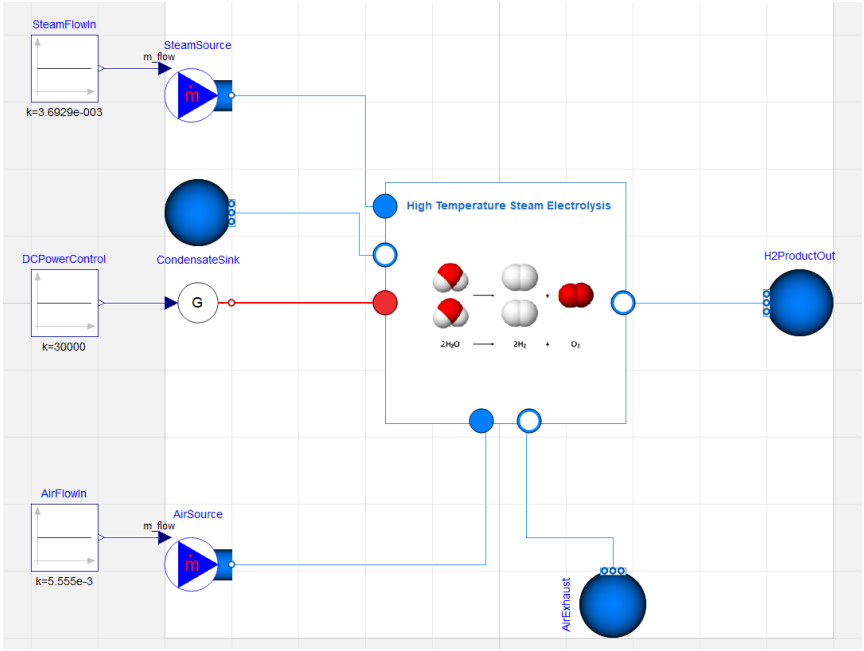

Figure 24. Dymola-based HTSE model.

4.2 Modeling Results

The dynamic HTSE model was compared with an equivalent Aspen HYSYS model and an Excel-based model, both of which are steady-state simulators. The effects of varying the DC power into the stacks were analyzed, and the results are presented below. Figure 25 shows the effect of varying the DC power (from 30 to 40 kWe) on the steam utilization. Increasing the DC power increases the total current and thus the amount of steam that is split. It is evident from the plots that the results of the Dymola and HYSYS models agree well with each other.

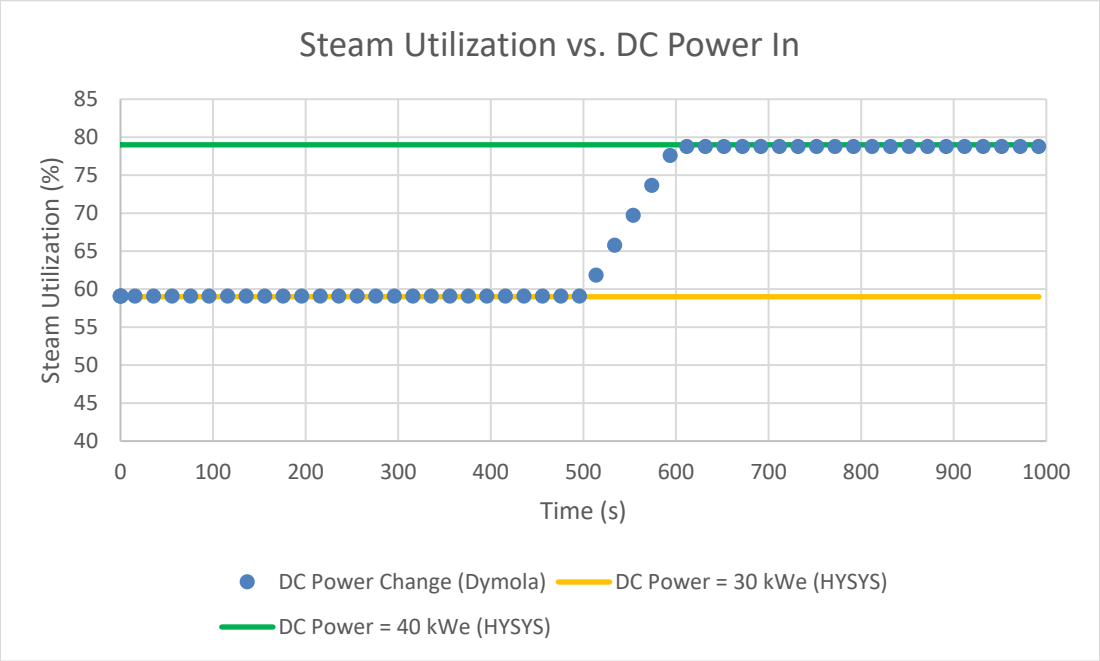

Figure 25. Effect of varying DC power (into the HTSE) on steam utilization.

In Figure 26, a similar comparison is drawn between the two models by displaying the hydrogen production rates. It should be noted that this is the net hydrogen production rate, which takes into account the amount of hydrogen recycled to maintain a certain composition at the cathode inlet stream. This comparison between the Dymola-based HTSE model and the HYSYS- and Excel-based models supports the verification of the developed dynamic model. As experimental data are currently unavailable, validation of the models was impossible. This will, however, be included in the future.

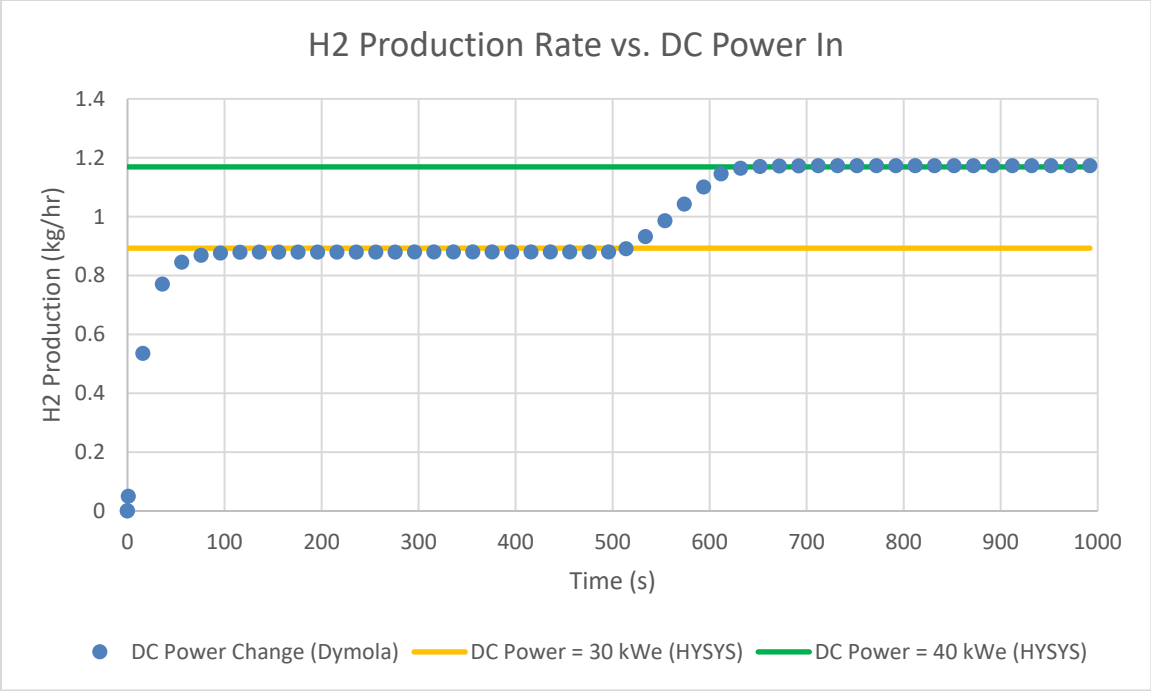

Figure 26. Effect of varying DC power (into the HTSE) on hydrogen production rates.

4.3 Additional Planned Work

Experimental analyses for the 30 kW system have been planned for the future. Once empirical data are available, validation of the developed models will be conducted. Additional planned work for the dynamic model entails the following:

- Develop a standalone heat exchanger model that would allow for condensation and cooling of a multispecies gas stream.
- Add control mechanisms to the HTSE model to ensure that changes in fluid flow rates and DC power occur in a proportional manner. This would enable the HTSE system to be coupled as a submodule to components as a part of an integrated system design.
- Modify the current model to allow for operating the SOEC in fuel cell mode. This would require the addition of several components and bypasses, as the sizes of the components used within the different operating modes vary.
- Add comments to the underlying code and push the models to the HYBRID repository.

5. CONCLUSIONS

The IES team at INL continues to develop modeling tools for analyzing physical experimental systems. The experiments within the DETAIL facility have been—and are intended to be—used to demonstrate practical dynamic applications of simulated nuclear heat generation. Through this work, the HYBRID modeling team is positioned to verify modeling efforts and provide those models to other IES teams (e.g., real-time optimization and digital twins).

The HYBRID modeling team at INL has successfully furthered the modeling of experimental systems at INL. When full-system experimental data become available, the HYBRID team will be prepared to exercise validation and verification of the modeled systems by using experimental data. The MAGNET facility model has been added and integrated with the existing TEDS facility model in the same manner as the physical experimental integration. An anticipated addition to the MAGNET system is the gas turbine power production loop, which has been modeled and integrated with the MAGNET and TEDS models.

HTSE modeling has progressed, anticipating a variety of SOEC stacks across INL's experimental facilities. The only major step required on this front is the development of an appropriate heat exchanger between TEDS and the various HTSE inlet streams. Anticipated use of this model includes a variety of SOEC stacks being tested at INL experimental facilities, as well as potentially in hydrogen hub activities. The new HTSE model supplements a pre-existing HTSE model within HYBRID.

6. ACKNOWLEDGEMENTS

This work was supported by the IES program at INL under DOE Operations contract no. DE-AC07-05ID14517.

7. REFERENCES

1. Frick, K. L. and D. Mikkelson (2022) "HYBRID," [updated 2022 April 6; cited 2022 April 13]. Available at: https://www.github.com/idaholab/HYBRID.
2. Frick, K. L., S. M. Bragg-Sitton, and C. Rabiti (2020) "Development of the INL Thermal Energy Distribution System (TEDS) in the Modelica Eco-System for Validation and Verification," INL/EXT-20-59195, Idaho National Laboratory. https://doi.org/10.2172/1668777.
3. Frick, K. L., S. M. Bragg-Sitton, and M. Garrouste (2021) "Validation and Verification for INL Modelica-based TEDS models Via Experimental Results," INL/EXT-21-64408, Idaho National Laboratory. https://doi.org/10.2172/1836100.
4. Kim, J. S., S. M. Bragg-Sitton, and R. D. Boardman (2017) "Status Report on the High-Temperature Steam Electrolysis Plant Model Developed in the Modelica Framework (FY17)," INL/EXT-17-43056, Idaho National Laboratory. https://doi.org/10.2172/1408745.
5. Dassault Systems (2021) "DYMOLA Systems Engineering [Internet]," [updated 2021 May 21; cited 2021 Nov. 16]. Available at: https://www.3ds.com/products-services/catia/products/dymola/.
6. Modelica Association (2020) "Modelica Standard Library [Internet]," [updated 2020 June 4; cited 2021 November 16]. Available at: https://github.com/modelica/Modelica.
7. Greenwood, M. S. (2017) "TRANSFORM - TRANsient Simulation Framework of Reconfigurable Models. Computer Software [Internet],"[updated 2017 Nov. 07]. Oak Ridge National Laboratory. Available at: https://github.com/ORNL-Modelica/TRANSFORM-Library.
8. Kim, J. S., R. D. Boardman, and S. M. Bragg-Sitton (2018) "Dynamic performance analysis of a high-temperature steam electrolysis plant integrated within nuclear-renewable hybrid energy systems," *Applied Energy*, vol. 228, pp. 2090-2110. https://doi.org/10.1016/j.apenergy.2018.07.060.

9. J. Mougin. (2015) “Hydrogen production via high-temperature steam electrolysis,”. *Energy*, pp. 225–253. https://sci-hub.se/10.1016/b978-1-78242-361-4.00008-x.
10. McBride B. J., S. Gordon, and M. A. Reno (1993) “Coefficients for calculating thermodynamic and transport properties of individual species,” NASA Technical Memorandum 4513. Available at: https://ntrs.nasa.gov/api/citations/19940013151/downloads/19940013151.pdf.